

ADVANCED X-RAY CHARACTERIZATION OF ULSI MATERIALS

THESIS

Presented to the Graduate Council of

Southwest Texas State University

in Partial Fulfillment of

the Requirements

For the Degree of

Master of SCIENCE

By

Anival Ayala

San Marcos, TX

December 2000

*This thesis is dedicated to my Father Victor Ayala and Mother Noelia Ayala for showing me that I can accomplish anything that I desired. I would also like to thank them for being there when I need them the most and I hope to do the same. Thanks Mom and Dad. I love you!*

## ACKNOWLEDGEMENTS

I would like to take the time to thank Dr Gutierrez, Dr Geerts, and Dr Michalk for being on my committee and reviewing my thesis. I would also like to thank again Dr Gutierrez for having the confidences in me to continue my education at SWT and giving me the opportunities to learn from him

I would also like to thank fellow graduates for teaching me the ropes around the Physics department at SWT, Ray Selestino and Eric Wittry

Also like to thank Dr Gutierrez's supporting crew for helping me out during some of the crisis that came: Mike Matheaus, Matt Langendroff, and Albert Teijerena. I would also like to thank Kevin Wiederhold for helping me out with maintaining the computers and the systems used in our research

I would also like to thank Tim Hossain for hiring me and letting me learn from him Thanks for being a good mentor and teacher. Also Allen Evans thanks for giving me a chance to work in Fab25 and also for being a great mentor Thanks for always backing me up.

Finally I would also like to thank Nadia Badillo for putting up with me through my most stressful time during my thesis. Thanks for being there and keeping me sane while I was writing my thesis I love you Nadia.

# TABLE OF CONTENTS

ACKNOWLEDGEMENTS.....	v
LIST OF FIGURES.....	vii
CHAPTER 1 INTRODUCTION.....	1
CHAPTER 2 FABRICATING TEST FILMS FOR ULSI AND OTHER DEVICES	
PHYSICAL VAPOR DEPOSITION.....	5
CHEMICAL VAPOR DEPOSITION.....	9
CHAPTER 3 PHYSICS OF ADVANCED X-RAY FILM ANALYSIS.....	19
BASIC X-RAY PHYSICS.....	19
BRAGG-BRENTENO DIFFRACTION.....	24
GRAZING INCIDENCES X-RAY DIFFRACTION.....	26
X-RAY REFLECTIVITY.....	30
CHAPTER 4 X-RAY DATA & RESULTS.....	42
CHAPTER 5 CONCLUSION.....	78
APPENDIX A.....	80
APPENDIX B.....	81
PUBLICATIONS.....	82
BIBLIOGRAPHY.....	83
VITA.....	84

## LIST OF FIGURES

Figure 1 Simple drawing of a Magnetron Sputtering.....	6
Figure 2 This is a simple drawing of a Dual Ion Beam Sputtering System.....	7
Figure 3 A Simple Prototype of a Thermal CVD Reactor.....	10
Figure 4 The schematics of the Novellus Altus system that is used to deposit Tungsten....	15
Figure 5 This is the wafer movement in the Altus CVD system.....	17
Figure 6 The Bremsstrahlung spectrum of a copper.....	21
Figure 7 Schematic of a Sealed x-ray tube.....	22
Figure 8 Bragg Diffraction of a crystal lattice.....	24
Figure 9 Powder diffraction $\theta/2\theta$ measurement.....	27
Figure 10 Grazing Incident Scan showing the movement of the scattering vector.....	28
Figure 11 Is a grazing incidence of the X-ray onto a sample and show the penetration Depth as a function of incident angle.....	31
Figure 12 The specular reflection of x-rays in a layered structure.....	33
Figure 13 Simulations of a 500 Å SiO <sub>2</sub> /Si and Ta/Si.....	35
Figure 14 500 Å Ta/Si film with 20 Å at interface Si/Ta and on Ta/air surface.....	36
Figure 15 Simulation of 500 Å Ta/Si with 20 Å roughness on Si compared with roughness on Ta.....	37
Figure 16 Simulation of Ideal 500 Å Ta/Si compared with 500 Å Ta/50 Å Ta <sub>2</sub> O <sub>5</sub> /Si.....	38
Figure 17 Simulation of 20 Å rough Si and Ta with ideal Ta <sub>2</sub> O <sub>5</sub> compared with Ideal 500 Å Ta/50 Å Ta <sub>2</sub> O <sub>5</sub> /Si.....	39
Figure 18 Simulation of rough Si/Ta <sub>2</sub> O <sub>5</sub> interface with ideal Ta compared to Ideal 500 Å Ta/50 Å Ta <sub>2</sub> O <sub>5</sub> /Si.....	40

Figure 19 Simulation of and Ideal 500A Ti/Si compared with Ideal 400 A Ti/100 A TiN/ Si.....	41
Figure 20 XRD scan of Si wafer/1000A SiO <sub>2</sub> /10A NiFe/100A Ta/300A NiFe/ 100A Ta...	44
Figure 21 XRD scan of Si wafer/1000A SiO <sub>2</sub> /10A NiFe/100A Ta/300A NiFe/ 100A Ta...	45
Figure 22 XRD scan of Si wafer/1000A SiO <sub>2</sub> /10A NiFe/100A Ta/500A NiFe/ 100A Ta...	46
Figure 23 XRD scan of Si wafer/1000A SiO <sub>2</sub> /10A NiFe/100A Ta/300A NiFe/ 100A Ta...	47
Figure 24 XRD scan of Si wafer/1000A SiO <sub>2</sub> /10A NiFe/100A Ta/300A NiFe/ 100A Ta...	48
Figure 25 XRD scan of Si wafer/1000A SiO <sub>2</sub> /10A NiFe/100A Ta/500A NiFe/ 100A Ta...	49
Figure 26 XRD scan of Si wafer/1000A SiO <sub>2</sub> /10A NiFe/100A Ta/200A NiFe/ 100A Ta...	50
Figure 27 XRD scan of Lucent Technologies 5000 A AlCu film.....	51
Figure 28 XRD scan of Lucent Technologies 500 A Ta/TaN film.....	52
Figure 29 XRD scan of AMD 300 A Ti film.....	53
Figure 30 XRD scan of AMD 5000 A Al/TiN stack film.....	54
Figure 31 GIXRD scan of Si wafer/1000A SiO <sub>2</sub> /10A NiFe/100A Ta/300A NiFe/ 100A Ta at 1 degree of incidences.....	55
Figure 32 GIXRD scan of Si wafer/1000A SiO <sub>2</sub> /10A NiFe/100A Ta/300A NiFe/ 100A Ta at 1.5 degree of incidences.....	56
Figure 33 GIXRD scan of Si wafer/1000A SiO <sub>2</sub> /10A NiFe/100A Ta/300A NiFe/ 100A Ta at 2 degree of incidences.....	57
Figure 34 GIXRD scan of Si wafer/1000A SiO <sub>2</sub> /10A NiFe/100A Ta/300A NiFe/ 100A Ta at 2 degree of incidences.....	58
Figure 35 GIXRD scan of Si wafer/1000A SiO <sub>2</sub> /10A NiFe/100A Ta/200A NiFe/ 100A Ta at 1 degree of incidences.....	59
Figure 36 GIXRD scan of Si wafer/1000A SiO <sub>2</sub> /10A NiFe/100A Ta/200A NiFe/ 100A Ta at 2 degree of incidences.....	60

Figure 37 GIXRD scan of Si wafer/1000A SiO <sub>2</sub> /10A NiFe/100A Ta/500A NiFe/ 100A Ta at 1 degree of incidences.....	61
Figure 38 GIXRD scan of Si wafer/1000A SiO <sub>2</sub> /10A NiFe/100A Ta/500A NiFe/ 100A Ta at 2 degree of incidences.....	62
Figure 39 GIXRD scan of Si wafer/1000A SiO <sub>2</sub> /10A NiFe/100A Ta/300A NiFe/ 100A Ta at 1 degree of incidences.....	63
Figure 40 GIXRD scan of Si wafer/1000A SiO <sub>2</sub> /10A NiFe/100A Ta/300A NiFe/ 100A Ta at 1.5 degree of incidences.....	64
Figure 41 GIXRD scan of Si wafer/1000A SiO <sub>2</sub> /10A NiFe/100A Ta/300A NiFe/ 100A Ta at 2 degree of incidences.....	65
Figure 42 GIXRD scan of Si wafer/1000A SiO <sub>2</sub> /10A NiFe/100A Ta/300A NiFe/ 100A Ta at 2 degree of incidences.....	65
Figure 43 GIXRD scan of Si wafer/1000A SiO <sub>2</sub> /10A NiFe/100A Ta/300A NiFe/ 100A Ta at 2 degree of incidences.....	66
Figure 44 GIXRD scan of Lucent Technologies 5000 A AlCu film.....	67
Figure 45 GIXRD scan of Lucent Technologies 500 A Ta/TaN film.....	68
Figure 46 1000A Cu film.....	68
Figure 47 This is a screen shot of REFS Mercury Software Shows model that was used to fit sample SWT 1-3.....	72
Figure 48 Screen Shot of REFS Mercury fitting the XRR data of SWT 1-3.....	72
Figure 49 This is a screen shot of REFS Mercury Software Shows model that was used to fit sample SWT 1-4.....	73
Figure 50 Screen Shot of REFS Mercury fitting the XRR data of SWT 1-4.....	73
Figure 51 This is a screen shot of REFS Mercury Software Shows model that was used to fit sample SWT 1-5.....	74
Figure 52 Screen Shot of REFS Mercury fitting the XRR data of SWT 1-5.....	74

Figure 53 This is a screen shot of REFS Mercury Software Shows model that was used to fit sample SWT 1-5 this has constraints on the Ta layers of 100A thick.....	75
Figure 54 Screen Shot of REFS Mercury fitting the XRR data of SWT 1-5 with Constraints on the Ta layers.....	75
Figure 55 This is a screen shot of REFS Mercury Software Shows model that was used to fit sample SWT 1-6.....	76
Figure 56 Screen Shot of REFS Mercury fitting the XRR data of SWT 1-6.....	76
Figure 57 This is a screen shot of REFS Mercury Software Shows model that was used to fit sample SWT 1-7.....	77
Figure 58 Screen Shot of REFS Mercury fitting the XRR data of SWT 1-7.....	77

# CHAPTER 1

## INTRODUCTION

The implementation of Integrated circuit (IC) technology has become pervasive in everyday life. In particular, high-end microprocessor and memory IC's are becoming faster and more powerful due to the fact that ever increasing numbers of ever smaller semiconductor devices are being packed into IC's of increasingly larger dimensions. The very rapidly decreasing size of features on an IC (presently at 0.18 microns) requires the implementation of new film materials in order to make the IC function properly. The presently used IC film materials (like aluminum, copper and many others) are generally failing in devices with dimensions that small. It is becoming very important to know which properties we can control to achieve the correct traits needed to build ULSI devices. Thus film property traits like grain size, crystal structure (phase), interfacial roughness, and density is now becoming very important characteristics in ULSI (Ultra Large Scale Integration) device design and fabrication.

Grain size has a large impact in several areas of ULSI fabrication. For example in an etch process the grain sizes can impact the rate a material etches away and also the quality of the device or structure left behind. Another area that can be affected by the grain size is the Chemical Mechanical Polish (CMP) process used for the fabrication of these devices. Again this also causes similar affects as in Etch where the grain size can

either slow down or even speed up the etch or polishing process of the materials involved.

In most ULSI devices electrical properties are important and the crystal structure plays a large role in these properties. The resistivity of a thin film depends on the crystal structure. The most striking example of the relation between crystal structure and conductivity is diamond and graphite. The former is an insulator (bandgap = 5.5 eV) while graphite is clearly a conductor. Both materials consist of solely carbon atoms. So by understanding, which preferred crystal structure gives you the correct electrical properties, you can improve the quality of your device. Another area that is also dependent on the crystal structure is the implant area. The implant area is where they put impurities into the semiconductor to get the right conductive properties needed to make ULSI devices. Which crystal structure is present depends on how far the implanted materials embed itself in the ULSI device. Thus, a very inconsistent crystal structure in the material before implant will result a very inconsistent implant depth. This could cause many undesired affects to the ULSI device or its a smaller components transistor.

Since the dimensions are getting smaller and some physical properties are becoming more important it is becoming equally important to find ways to measure these physical properties. There are many techniques that can be used to measure certain physical properties of the materials used in ULSI devices. X-rays can be used to gain much of the information that is needed to understand the properties of film materials useful for ULSI devices. Even though x-rays can give an abundance of information it is not the holy grail of measurements techniques (for example x-rays are not surface

sensitive and cannot be focused to sub micron areas). It is however complementary to other analysis techniques.

X-rays are used in almost every discipline of science and engineering. In the medical field, x-rays are used to take pictures of the human body to detect skeletal injuries. Where the bones tend to adsorb x-rays, the soft tissue is relatively transparent. In aerospace, they use x-rays to hunt down stress fractures in the body or wing of the aircraft. So for ULSI devices it can also be used since the devices are on the order of several microns in size.

There is not one specific x-ray analysis method that gives you all of this information. There are three different techniques that can be used to get the desired information. The three techniques are Powder X-ray Diffraction, Grazing Incident X-ray Diffraction (GIXRD), and X-ray Reflectivity. Each of these techniques uses the properties of x-rays in a very similar way and will be discussed later in the chapters to come

Along with the X-ray methods there will be some discussion over the methods used to grow the films that were analyzed. The methods are Physical Vapor Deposition, Chemical Vapor Deposition, and Dual Ion Beam Sputtering. Each deposition takes place in a controlled atmosphere of a vacuum chamber. The only difference is in the deposition pressure. Most of these films that are used in this analysis were fabricated at the Physics Department at Southwest Texas State University and a small number were fabricated at Lucent Technology and Advanced Micro Devices.

I will present examples of how these x-ray analysis methods can be used to detect crystalline phase, thickness and interface roughness for a wide variety of film materials especially those vital for ULSI devices.

## **CHAPTER 2**

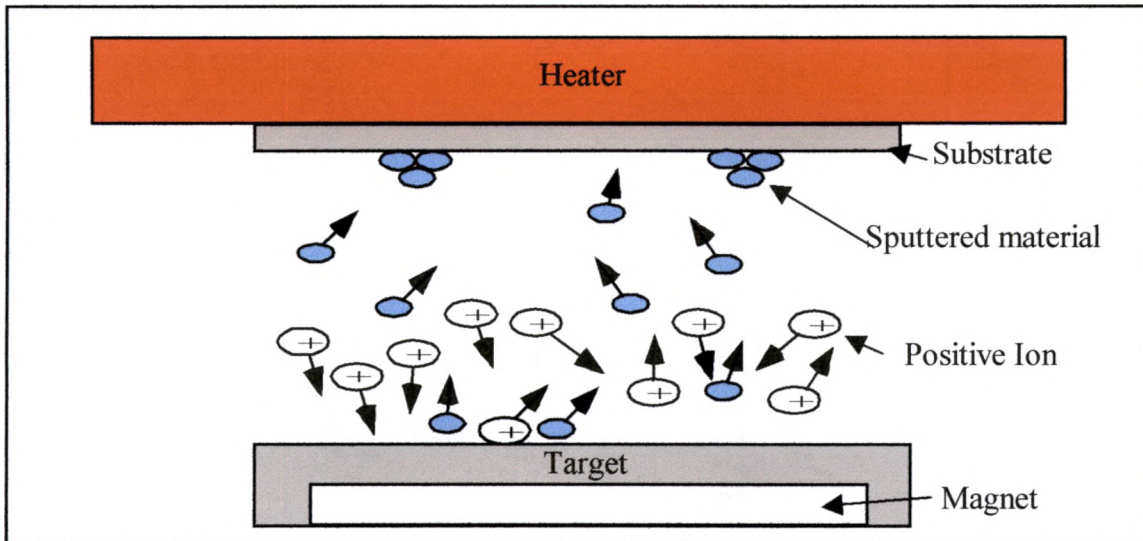
### **FABRICATING TEST FILMS FOR ULSI AND OTHER DEVICES**

#### **PHYSICAL VAPOR DEPOSITION**

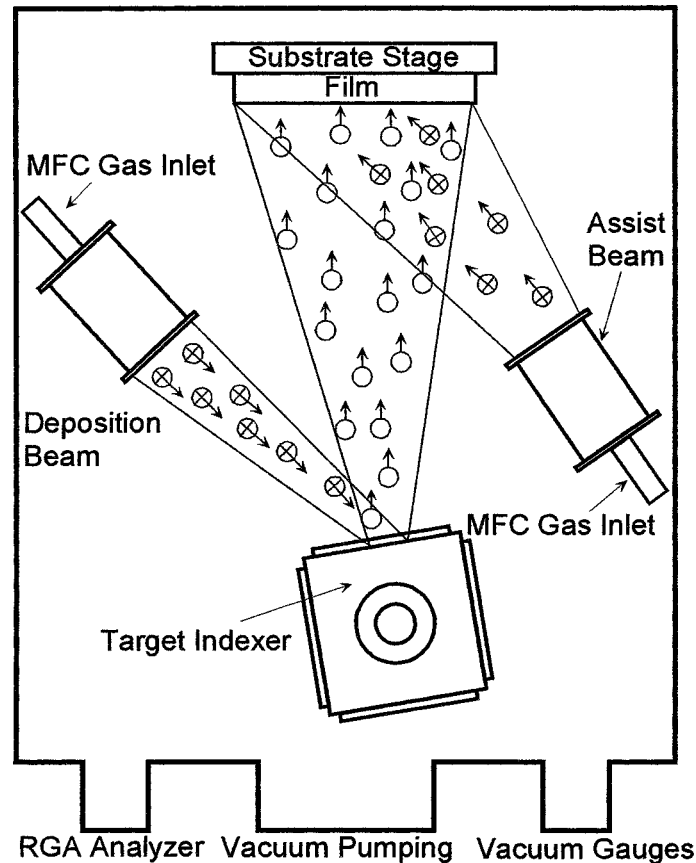
Most test films used in this study were made by physical vapor deposition or sputtering. Sputtering is a method of depositing films, which has been known since 1852 (Ref #1, p xx). Since the 1900 the advancements in vacuum techniques and the availability of ultra-high purity gas, have made the semiconductor industry accept this method of deposition. The Sputtering process takes place in a vacuum chamber at operating pressures between 10-100 mtorr ( $1.33 \times 10^{-3}$  Pa). The ultimate base pressure of the vacuum system before deposition is in the range of  $10^{-6}$  torr ( $1.33 \times 10^{-4}$  Pa) to  $10^{-8}$  torr ( $1.33 \times 10^{-6}$  Pa). There are several types of sputtering systems that were used to deposit the films that I have study. One is the Magnetron sputtering and the other is the Dual Ion Beam Sputtering (DIBS). Figure 1 shows a basic drawing of Magnetron sputtering process

Figure 2 shows a dual ion beam sputtering system. This system is very similar to a magnetron sputtering system. The difference between the DIBS and the magnetron sputtering system is that in the DIBS an ion beam generated by a Kaufman ion source

performs the sputtering process. As for the magnetron system the sputtering is done by a plasma created between the substrate and the target. This plasma is created by an electrical potential difference applied between substrate and the target. This attracts the positive argon ions to the target material. Both of these systems are held at typical deposition pressures of  $4 \times 10^{-4}$  torr (0.0533 Pa) to .01 torr (1.333 Pa)



**Figure 1 Simple drawing of a Magnetron Sputtering**



**Figure 2 This is a simple drawing of a Dual Ion Beam Sputtering System**

The Sputtering process occurs when charged atoms of argon bombard a target containing the material for deposition (Ref #2, p.xx). This causes the target to erode because target atoms will be knocked off (sputtered) the target surface into the vacuum and will condense elsewhere in the vacuum system, in particular on the substrate. For magnetron and ion beam sputtering, a base pressure around  $10^{-6}$  to  $10^{-8}$  torr ( $1.33 \times 10^{-4}$  to  $1.33 \times 10^{-6}$  Pa) is required. This is necessary in order to avoid the incorporation of impurity atoms from the vacuum residual gas in the films. Once a low base pressure is obtained argon gas is led into the chamber. The sputter pressure is typically in the lower mtorr range. Some of the argon atoms are ionized. These argon ions will be accelerated to the negative target for sputtering, while secondary electrons stripped from the Argon atoms generate more argon ions to sustain a plasma. This causes a plasma to form

between the target and the substrate. The electric potential between the target and the substrate can be a DC voltage or an RF (radio frequency) voltage. There are several ways to look at each type of power supply. DC voltage power supplies are used to produce a plasma for sputtering metal or conducting target materials. In the case of using a non-conducting material the DC power has a tendency to build a charge sheath on the target surface inhibiting a stable plasma for sputtering. RF power supplies eliminate this problem for insulation targets, but RF power uses very high voltages where DC can use rather low voltage for example 120 for DC versus 210 volts for RF. For further information on DC and RF sputtering refer to Raymond Selestino's (MS Physics, 98) thesis *Fabrications and Analysis of Ferromagnetic Cobalt Iron Metal Alloy Multilayers* (Ref #3, p xx) in his chapter on sputtering.

DC and RF sputtering deposited most of the test films used in this study. The test films came from several different sources such as SWT Physics Department, Lucent Technologies, and Advanced Micro Devices. Each source used either DC or RF sputtering to deposit the films.

The first set of films is a multiplayer film of Tantalum and Permalloy (Nickel-Iron). Robert Dail (MS Physics, 97) created this set and used a Commonwealth Scientific Corp. (CSC) sputtering system. CSC is now known as Veeco. These films have a complicated structure or pattern. The Tantalum and Permalloy consist of a Silicon substrate with a ~100nm Silicon Oxide. On top of the oxide is a 1 nm thick Permalloy seed layer. A Tantalum layer of 10 nm is then deposited on top of the Py seed layer. Then there is an active layer of Py which has a varying thickness of ~10nm to ~50nm. The

films are capped with a 10nm thick Tantalum layer. Each of the eight films in this set was deposited on 15X15 mm silicon.

Another set of films was made at Lucent technology. These films are much simpler than the previous films from Robert Dail (Ref #4, p. xx). All films are single layer films on silicon. Each sample used was taken from a full 200 mm wafer, which was deposited by several different materials. The four different films I looked at are a single layer of ~50nm Tantalum, ~50 Tantalum Nitride, ~500nm of Al with a .05 percentage of copper, and ~50nm of Titanium Nitride. Each one of these films was deposited by a PVD method either being DC or RF sputtering.

## **CHEMICAL VAPOR DEPOSITION**

Chemical vapor deposition has become a very widely used and preferred deposition method for a large range of materials. The reason this is occurring is that there are many modifications of the CVD process that provide alternative energy sources such as plasma or optical excitation to drive the chemical reactions. These new modifications allow the deposition to occur at lower temperature.

To better understand the CVD process let me start with a very simple model of a CVD reactor. The reactor is a rectangular tube that has a gas inlet on one end and a gas exhaust on the opposite end of the reactor. On the inside of the reactor you need a susceptor that holds the wafer and also is able to heat up the wafer.

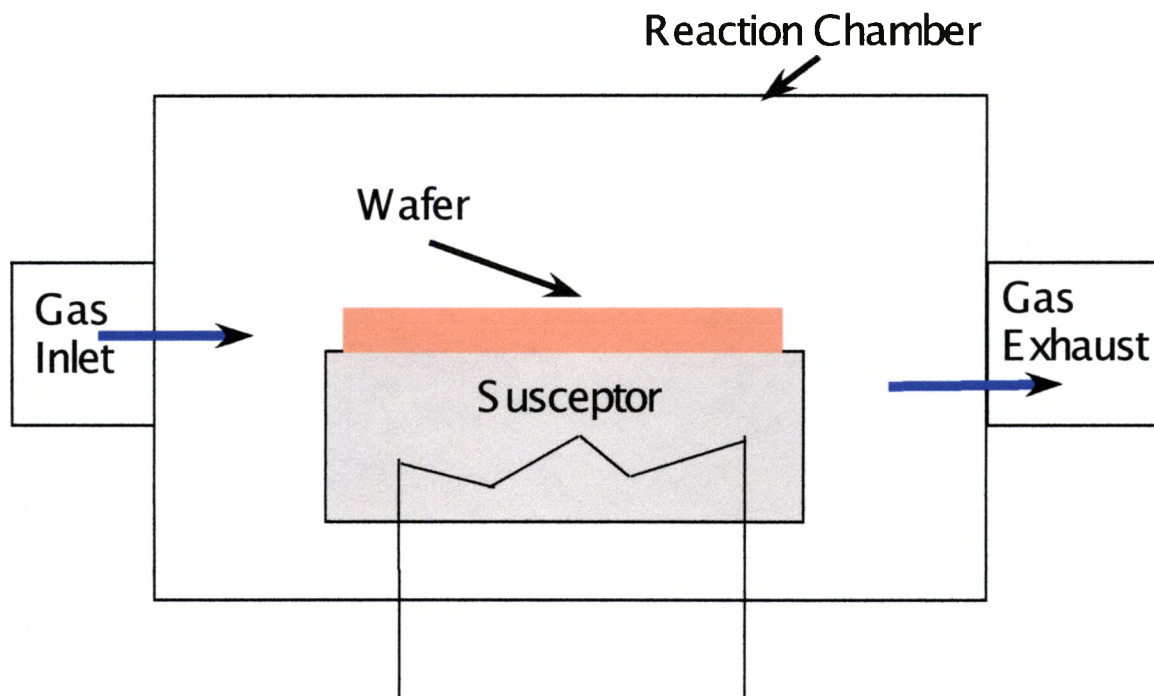
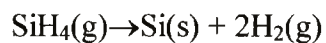


**Figure 3 A Simple Prototype of a Thermal CVD Reactor**

The way this simple prototype of a thermal CVD reactor works is by flowing the reactant gas in the gas inlet and letting it flow through the tube and to the gas exhaust. As the gas travels through the tube the reaction takes place near the wafer due to the heat that is being produced by the susceptor. An example of this type of process is the deposition of polycrystalline silicon. The gas that is used to deposit poly-silicon is Silane gas ( $\text{SiH}_4$ ) that starts to breakdown in the presence of heat and carrier gas such as molecular hydrogen. So the reaction that takes place in our prototype reactor is



Equation 2.1

where (g) stands for gas phase and (s) stands for Solid.

Stephen A Campbell best states the steps of the CVD process:

1. The transport of the precursors from the chamber inlet to the proximity of the wafer,
2. Reaction of these gasses to form a range of daughter molecules,
3. Transport of these reactants to the surface of the wafer
4. Surface reactions to release the material desired
5. Desorption of the gaseous byproduct
6. Transport of the byproducts away from the surface of the wafer
7. Transport of the byproduct from the reactor (Ref #5, p. xx)

The simple reactor that I described earlier is just one type and there are other types of CVD processes; for example, Atmospheric CVD of Dielectrics, Low Pressure CVD of Dielectrics and Semiconductors in a hot wall system, Plasma Enhanced CVD of Dielectrics, and Metal CVD. Each of these uses the very similar mechanism of a gas that reacts at the wafer surface due to high temperature. The only difference between all of these processes is the pressure in the chamber where the reaction takes place.

Atmospheric CVD of dielectrics was used in the early stages of the semiconductor industry due to its large reaction rates and its simplicity of the CVD system (Ref #6,p. xx). As the name describes, the system or CVD process takes place in atmosphere. The only draw back was that uniformity was very poor. As the industry started growing so did the knowledge of the CVD systems. Semiconductor engineers started to realize that it was easier to produce a good uniform film at low pressures. So the introduction of Low Pressure CVD systems was used in growing these dielectric and semiconductor films. There are two types of reactors and they are a hot walled reactor and a cold walled reactor. In the hot walled reactor the walls of the chamber are kept at a constant temperature that is relatively close to the susceptor temperature. The hot walled reactor has an advantage of uniform temperature across the reactor. As for the cold walled

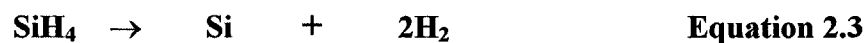
reactor the walls of the chamber are not heated and are usually kept at room temperature. Although this method has poor temperature uniformity, the cold walls help in reducing the deposition on the chamber walls that can contribute to flaking (particulate generation) that can cause serious damage to ICs. The operating pressure is  $\sim 10$  to 300 mtorr (1.33 to 40 Pa). The benefit of this low pressure is that the reaction temperature is lowered considerably. The only downfall to this is that since the deposition rate is dependent on the temperature and the rate decreases as the temperature decreases, the deposition rate of low pressure CVD is typically lower. In many applications, it is necessary to deposit films at very low substrate temperatures. (Ref #7, p. xx)

Plasma Enhanced CVD of dielectric is one of those processes that enable you to deposit films at very low substrate temperature. For Example,  $\text{SiO}_2$  over aluminum or  $\text{Si}_3\text{N}_4$  as a capping layer over GaAs are very common PECVD processes (Ref #8, p. xx). Again this process still depends on a thermal reaction of a gas on a heated wafer. In this system the plasma is used to help the reaction since the goal is to deposit at lower temperatures. As Campbell states that "Plasma enhanced deposition CVD systems have the added advantage of using ion bombardment of the surface to provide energy to the adspecies to allow them to diffuse further along the surface, without substrate temperature. (Ref #9, p. xx) There are three different types of PECVD systems, i.e. the Cold wall parallel plate, the hot wall parallel plate, and the after glow. Each of these systems uses RF power to excite the plasma in the chamber. The frequency chosen is normally set to less than one kHz, but in certain cases the power can increase much higher. This deposition pressure of the dielectric using PECVD is usually at  $\sim 10$  – 30 Torr due to the mean free path. If the

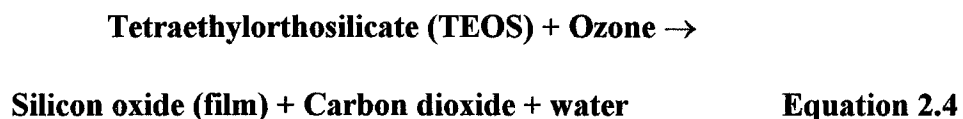
pressure is low and thus the mean free path is large you will get very poor step coverage since you are sputtering more material from the wafer

The last type of CVD process is Metal CVD. This type of CVD process uses most of the described systems to deposit a film. For example, the Tungsten deposition is a thermal CVD process

Some of the test films were deposited by using similar CVD processes that were described earlier. I mention earlier about the actual systems where CVD processes take place. Let me now talk about the reactions that take place inside the reactors. There are two types of CVD reactions. One is the decomposition of one precursor and the other is the combination of two or more reactants. An example of a single decomposition is when Silane reacts when the temperature is between 600-1100° Celsius and produces a silicon film and hydrogen gas waste by-product.



This CVD reaction is very widely used in the Semiconductor Industry as an initiation step for depositing tungsten films. An example of a combination of two reactants is when TEOS (Tetraethylorthosilicate) and ozone react to produce a silicon oxide film and leaves carbon dioxide and water. This reaction occurs between 300-500°C



This is also a widely used process in the semiconductor industry as a dielectric for the IC. Several of the test films I have studied were made with the same CVD process.

A tungsten film on silicon oxide is one of the films I used in this study. The tungsten was deposited by a basic thermal CVD process. This process is a little more complicated than the silicon or TEOS film processes. The tungsten and TEOS films were deposited at AMD (Advanced Micro Devices) using a Novellus Altus CVD tool. This tool is a cold wall reactor with five stages for a thermal deposition. The figure above shows the basic schematics of the Dual Altus. There are two load locks that hold the wafer cassettes to allow the robot arm to transfer the wafer to the reactor chamber. Once the wafer is in the reactor chamber it is cycled through the deposition process. Depending on the process the chamber will either have a plasma or not have a plasma during deposition. In the case of Tungsten deposition the plasma is only on during a clean not during the tungsten depositions. Thermal deposition is when the only mechanism is the heating pedestal. There is no plasma that occurs during this process. The Altus operates at ~40 Torr and heats the wafers to ~400° C. At each of the substrate pedestals there is a showerhead that brings the gases into the chamber. The Altus is set up to deposit 1/5<sup>th</sup> of the process at each pedestal. Tungsten deposition occurs when several reactions all taking place in a sequential order.

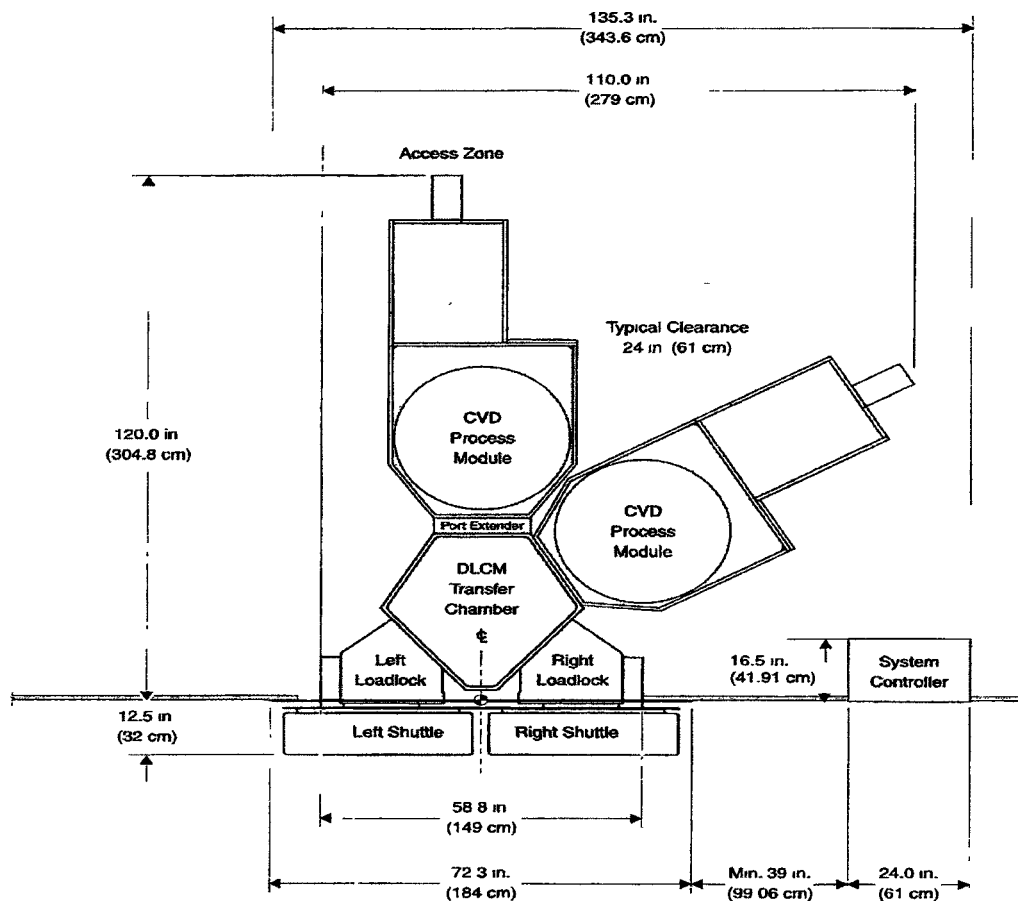
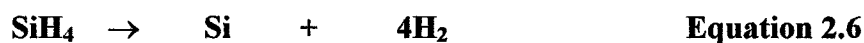
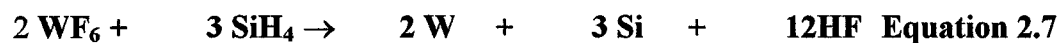


**Figure 4** The schematics of the Novellus Altus system that is used to deposit Tungsten

The first reaction is the Silane reaction with Hydrogen to form a thin layer of Silicon on the wafer surface.



This reaction is done to ensure that the tungsten adheres to the wafer. Then the next reaction is a combination of Tungsten Hexafluoride and Hydrogen to react with the thin layer of Silicon that leaves behind the desired Tungsten film.





This all occurs at the first station and 1/5<sup>th</sup> of the Tungsten is deposited on the wafer and then moved to the next station and the next wafer enter the chamber and the process repeats on the first station but on the second through fifth stations the process changes. The Silane is removed so that the only reaction is the Tungsten Hexafluoride and the Hydrogen that react to give the Tungsten film. The figure below shows the wafer movement through Altus system.

The wafers start in either the left or right shuttle. The shuttle let you load up to four cassettes on the tool. Each cassette holds up to twenty-five wafers. When the system is ready it loads up a cassette in each of the load locks. Whichever cassette is loaded first is the one that get processed first. So as soon as the load lock and the transfer chamber are at equal pressure then the robot are is ready to grab a wafer and transfer it into the reactor chamber. Then the first wafer get the first part of the process and when that is finished the wafer get indexed over to the second station and a new wafer enters the reactor chamber. This cycle takes place until all the wafers are processed. After the wafer has gone through each station in the reactor chamber it is set in a cooling station in the transfer chamber. When the wafer has had enough time to cool the robot arm picks up the wafer and puts it back into the cassette. After each wafer goes through this process and get placed back into the cassette then the load lock closes and starts to vent to bring the wafers back out to the clean room. Most of the CVD tools follow this same wafer movement during the process

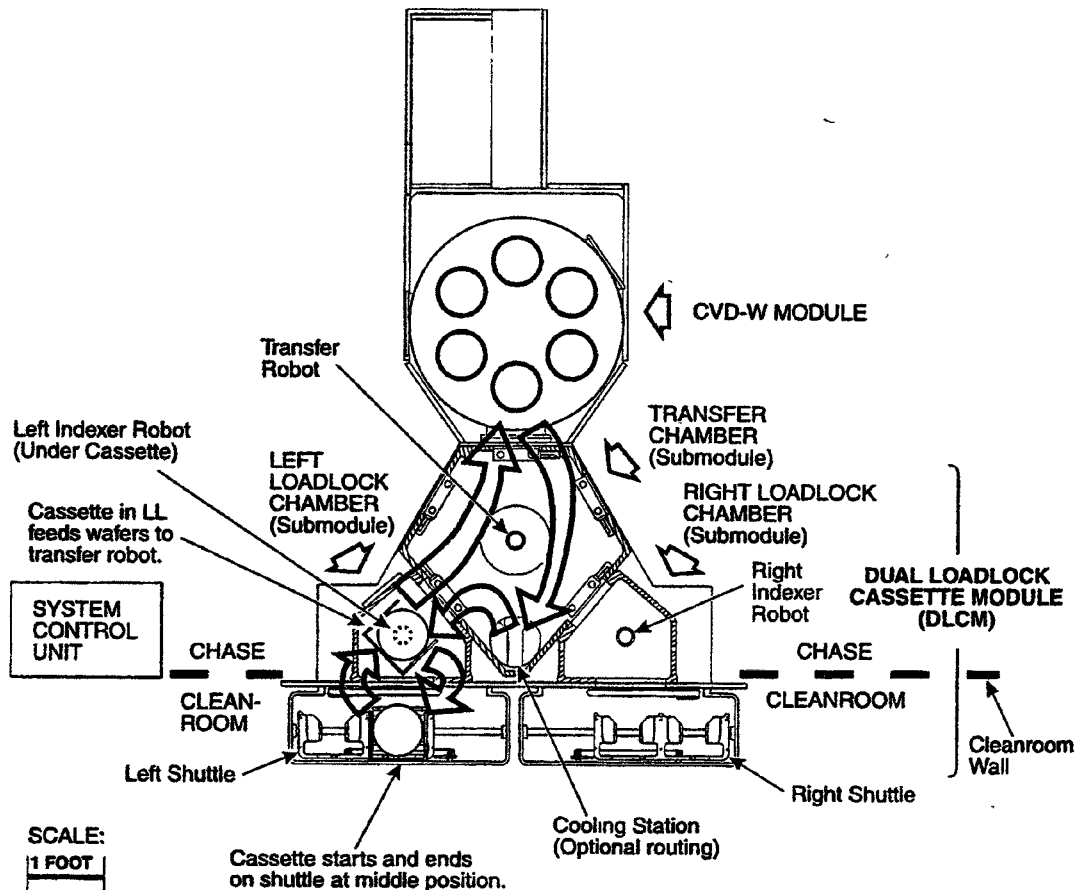


Figure 5 This is the wafer movement in the Altus CVD system

As I described the wafer movement for a tungsten process it is also the same for the dielectric process. For this process the gas used is called TEOS (Tetraethylorthosilicate). This gas breaks down to produce Silicon Dioxide. This process is different from the tungsten process, in which, there is a plasma present during the deposition of the silicon oxide film. The gases involved in this process are TEOS and Ozone, which react into silicon oxide, carbon dioxide and water.



The operating temperature for this process is 300-500° C This deposition process is an important part of creating ICs. It is used to separate metal contacts or metal lines to keep them from shorting out the circuit All of the different types of depositions that I discussed in this chapter are widely used in the semiconductor industry And since the deposition is a very important part in making IC's it is also important to know all the characteristics of the films that are being produced by these processes.

## CHAPTER 3

### PHYSICS OF ADVANCED X-RAY FILM ANALYSIS

A German physicist, Roentgen discovered x-rays in 1895. The reason they were called x-rays was due to the unknown characteristics at that time. Now the characteristics of x-rays are very much known today. X-rays are high-energy electromagnetic radiation with a short wavelength. X-rays can be described in two ways, as a wave or a particle of energy. When you think of x-rays as a wave you picture an oscillating electric field and at right to this field an oscillating magnetic field. By looking at an x-ray as a particle it is then called a photon, this is where it draws its similarities to light. All electromagnetic radiation is characterized either by its wave character using its wavelength  $\lambda$  and its frequency  $\nu$  or by its photon energy  $E$ . (Ref #4, p. xx). The following equations represent the relationship between these quantities:

$$\nu = c/\lambda \qquad \text{Equation 3.1}$$

$$E = h\nu \qquad \text{Equation 3.2}$$

Where  $c$  is the speed of light and  $h$  is Planck's constant. Since light can be described as electromagnetic radiation as well as x-rays, they only differ from each other by the wavelength size. Visible light has a larger wavelength (3800 - 7900 Angstroms) compared to x-ray wavelengths (0.5-2.5 Angstroms). This large of difference in the wavelength also impacts the photon energy available. Optical light's larger wavelength results in a lower photon energy, while x-rays the small wavelength translates to have much larger photon energy. To calculate the photon energy of light and x-rays you would need to combine equation 3.1 and 3.2.

$$E=hc/\lambda=1238.9/\lambda \text{ eV}$$

Equation 3.3

Then by plugging the correct constants and the wavelength for light and x-rays you can get the photon energy. For light the photon energy is  $\sim .002$  keV and for x-ray the photon energy is  $\sim 8.26$  keV. Having such a small wavelengths is very important to x-ray diffraction.

X-rays can be produced by rapidly decelerating any electrically charge particle that has sufficient kinetic energy. Electrons are these electrically charged particles that are used to produce x-rays. When the electrons collide with the element, for our case copper, a spectrum is obtained as in figure 3 1. This spectrum consists of a continuous band of radiation known as Bremsstrahlung or white radiation. Then superimposed in the Bremsstrahlung spectrum are discrete peaks of varying intensities.

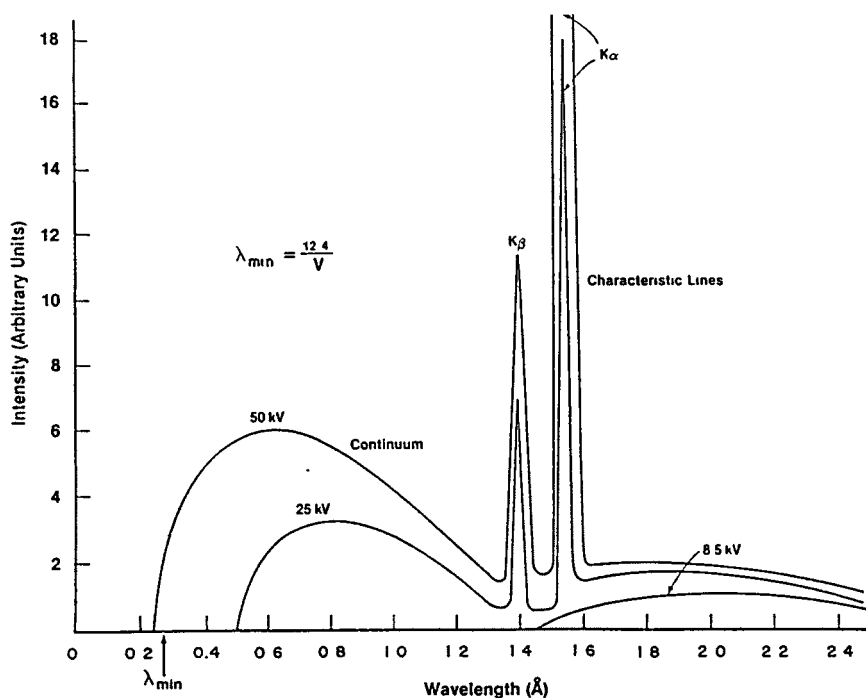


**Figure 6 The Bremsstrahlung spectrum of a copper**

The continuous spectrum is produced by the deceleration of the electrons as they hit the copper target or any other type of target material

There are three devices that can be used to produce x-rays. an evacuated tube, a rotating anode source, and synchrotron light source. The evacuated tube works as follows. In the sealed tube you have two metal electrodes. One is your source of electrons the cathode and the other is the anode or target material. By maintaining a high potential voltage between the anode and the target, electrons are accelerated to the anode or target material that is used to produce the x-rays. The potential is on the order of –30 to –100 KeV this potential difference will accelerate the electrons towards the positively charged anode. When the electron hits the target material two reactions occur. One of the reactions is to give off an x-ray the other is the larger reaction of the two and it is in

the production of heat. All of this occurs in a sealed tube that has been partially evacuated to increase the mean free path of the electron as it travels from the cathode to the anode. At the point of impact, a continuous spectrum of x-rays with different wavelengths, also called Bremsstrahlung x-rays, is produced in all directions (Ref 9,p.xx). This is another similarity to light where as light has different wavelengths that make up the white light. X-rays also have a so-called white x-rays which indicate many different wavelengths of x-rays. The sealed tube is a great method in producing x-rays but you are limited to only 2 kilowatts of power that can be produced by the tube. The reason is that you start running into problems in removing the heat that is created from the electron deceleration. So the cooling system cannot keep up with the rate that the heat is created. Another method or possible solution is to use a rotating Anode source.

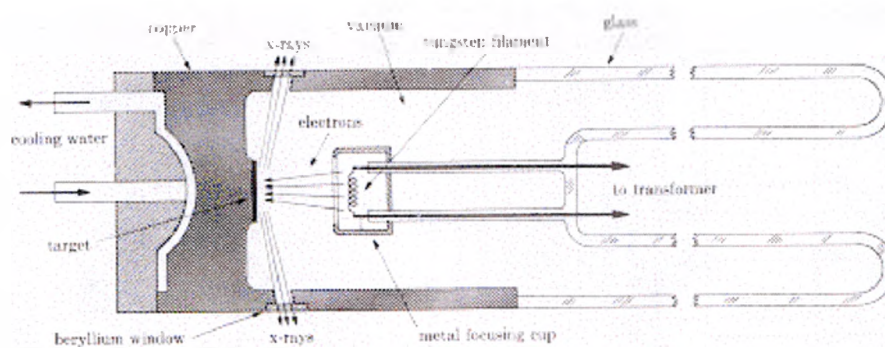


**Figure 7 Schematic of a Sealed x-ray tube**

A rotating anode works in a similar way the sealed tube does. A difference is that in the rotating anode, the target is not placed in a sealed tube. A rotating-anode is in a chamber that is kept under vacuum at all times. The production of x-rays is the same way that occurs in a sealed tube. In the rotating anode as the name states the anode is rotating so that the electrons will hit the anode each time at a different place, this way the heat is distributed over a larger area and cooling of the target is easier. This allows the use of

higher potentials between the cathode and the anode. The rotating anode can reach a power level 5 to 10 times higher than a sealed tube. The only downfall to this method is that there is a considerable amount of down time due to the vacuum and the moving parts involved in the source.

There is a third method that can be used to produce x-rays and that is in a Synchrotron. This method takes a lot more effort to produce the x-rays, but they x-rays are very strong and have a very small wavelength which is a very desirable for many types of applications. Again this method takes a large amount of area and effort to produce the x-rays. I was not able to consider this method since there is only a few areas in the United States that house this type of x-ray production.

I was able to work with two of the three types I mentioned. They were the sealed tube and the rotating anode. Both tools were built by Bede Scientific. The Sealed tube tool was a Bede 200 and the Rotating anode was a Bede D3 system. Most of my data was taken for the Bede D3 system. The Bede 200 is located at Southwest Texas State University in the Physics department. As for the Bede D3 system it is located in Advanced Micro Devices in Austin, TX inside PCAL (Physical Chemical Analytical Labs) I was trained on the Bede 200 system. Then I was hired due to my training on the Bede 200 to run AMD's Bede D3 system. So most of my data was gathered from the D3 system at AMD. Before I present my data let me give you some information about the three different techniques that I used to analyze these films.

## BRAGG-BRENTENO DIFFRACTION

When a periodical array of objects each scatter radiation coherently, the concerted constructive interference at specific angles is called diffraction. (Ref #4, p. xx) There were many early attempts to understand the duality of the characters of x-rays, as a particle and wave. But many were frustrated by experimental difficulties that came with the very short wavelengths of X-rays. Max von Laue in 1912 was able to confirm the wave character of the x-rays by diffraction experiment from a single crystal. From this experiment a new field of X-ray Crystallography arose. Max von Laue described x-ray diffraction of a single crystal with three-vector dot-product equations (Ref #4, pXX). Then in 1913, William H. Bragg and his son William L. Bragg developed a new way to understand and predict the x-ray diffraction from crystals.

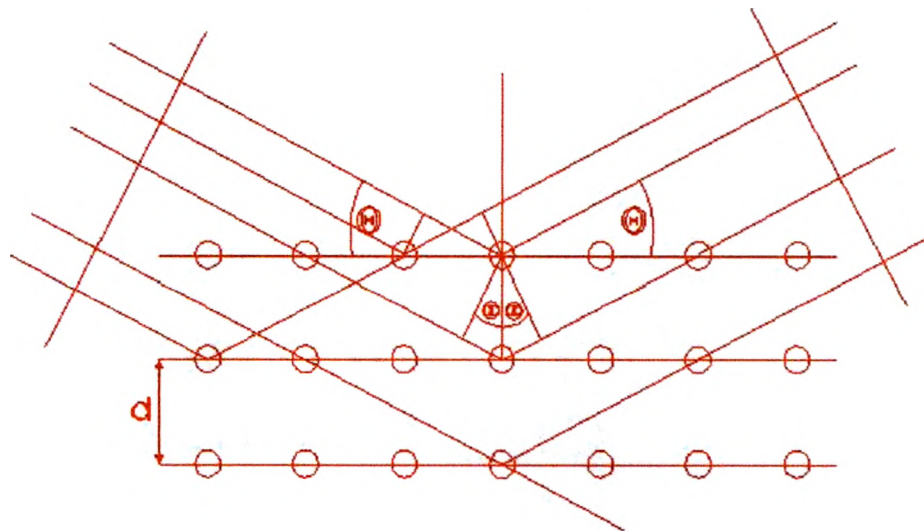


**Figure 8 Bragg Diffraction of a crystal lattice**

Henry and Lawrence Bragg simply used a 2-D diagram of a crystal lattice where the X-ray beam comes in from the left and reflects or diffracts towards the right. The reflection

takes place at each lattice. From this simple view of x-ray diffraction H. & L. Bragg were able to derive their equation known as the Bragg Equation:

$$n\lambda = 2d_{hkl}\sin\theta \quad \text{Equation 3.4}$$

where  $n$  is an integer,  $\lambda$  is the wavelength of the incident x-ray,  $d$  is the distance between adjacent planes, and  $\theta$  is the angle of incidence as shown in Fig. 3.2. Even though von Laue's description was heavily mathematical the Bragg equation simplified the math by using the analogy of reflection. Based on some of the books that I've read say that there is third description by P. P. Ewald. Ewald's description is called "reciprocal lattice" or "reciprocal space." Ewald's method is useful because it is able to predict the angle and  $d$ -spacing for any diffraction plane.

The Bragg-Brentano diffraction technique is used to determine what the material is and what the crystalline phase is present. It is a simple measurement. The method has only two moving motor that are linked together in a 1 to 2 ratio. These motors as in the D3 Bede system are the Axis 2 and the detector. The Axis 2 motor rotates the sample in either degrees or in Arc-seconds. Figure 3.3 show a basic setup of powder diffraction. It has a source that produces x-rays and they head down the system towards the Sample that is being measured. As the x-ray beam diffracts off the sample the x-ray are now on their way to the detector. In front of the detector there is a scatter shield and some slits that are used to filter out any stray x-rays. The detector and the Sample axis (axis 2) have to keep a  $\theta/2\theta$  relation in order to pick up x-rays that satisfy Bragg's Law.

This measurement is a very useful technique because the scans are fast and give you a lot of information. Powder diffraction data gives you information on what material is present in the IC, what crystal structure are present in the IC, and it also lets you know if the film is textured. To figure out what material is present in the sample you would need a little bit of information about the sample. In most cases you already know what the material is, that has been deposited on the wafer. By knowing this much you can then go to a database that has been collected by ICCD (International Crystallography Characterization Diffraction). You would then use the database to search match the right element to your data. By doing this you confirm that you have the material you deposited and also what crystal structure is present in the film. Sometimes it is not possible to determine the crystal structure from the powder diffraction data. Another technique that can be used to maybe confirm the material would be Grazing Incidences X-ray Diffraction (GIXRD).

## **GRAZING INCIDENCE X-RAY DIFFRACTION**

Grazing Incidences X-ray Diffraction (GIXRD) is a very useful technique that compliments powder diffraction. GIXRD can also be explained by or related to Bragg's Equations. As Powder Diffraction uses the simple idea of the angle of incidence is equal to the angle of diffraction, so does GIXRD. In Fig. 3.4 it shows the relation between the sample and the detector is shown.

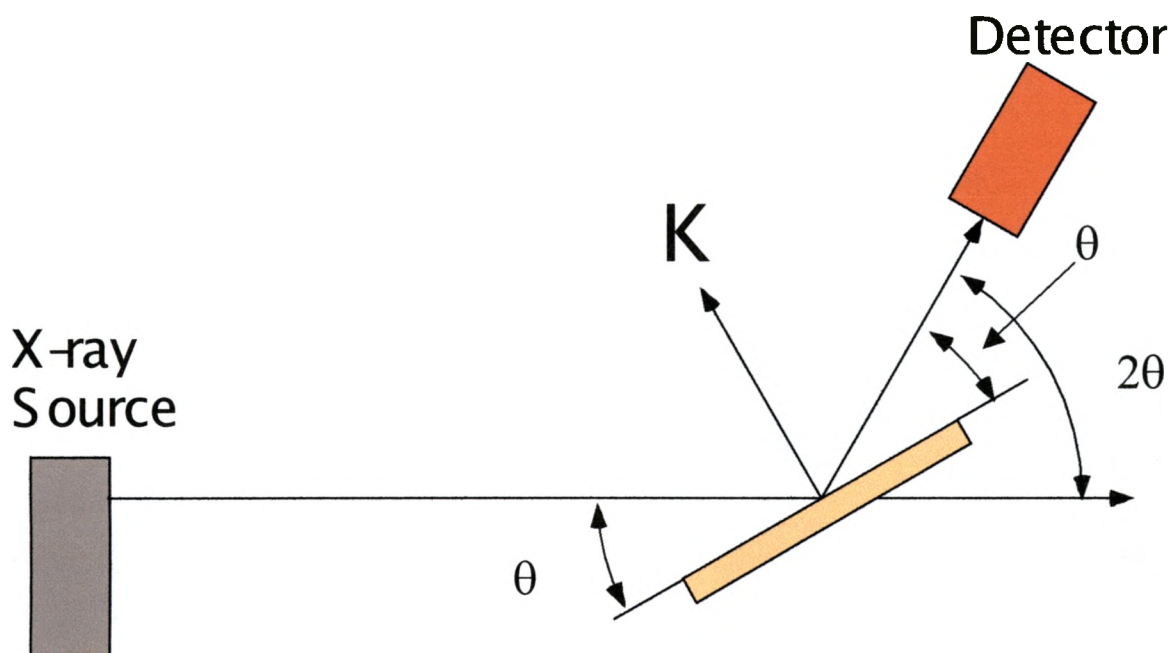


**Figure 9 Powder diffraction  $\theta/2\theta$  measurement**

As the x-ray comes into the sample at an angle of  $\theta$  it also reflects or diffracts at angle of  $\theta$ . So to be able to pick up the diffracted peak from the sample you would need to set your detector at double the angle of incidence as Fig 3.3 illustrates. The only thing is that instead of having a  $\theta/2\theta$  relation where the sample moves at  $\theta$  and the detector moves at  $2\theta$ . The detector only moves along the  $2\theta$  and the sample stays at a fixed angle  $\alpha$ . The  $2\theta$  movement by the detector is the normal movement in as is a Bragg-Brentano Diffraction.

The incident x-rays is then coming into the sample at this fixed angle  $\alpha$ . By doing this the x-ray penetration depth is very shallow compared to the powder method. In the powder method the x-rays tend to penetrate all the way through the sample. This makes it difficult to follow the structural variations as a function of depth. So by then having a fixed angle  $\alpha$  you are then controlling the depth the x-ray can penetrate into the sample.

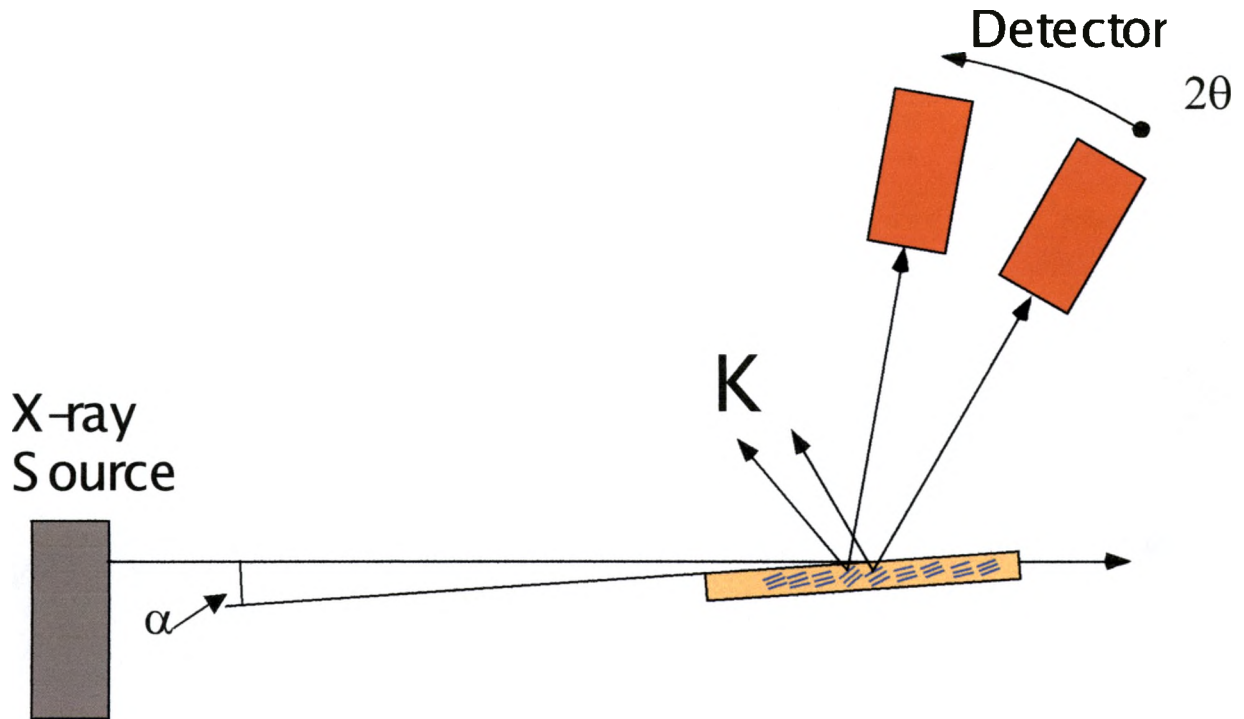


**Figure 10 Grazing Incident Scan showing the movement of the scattering vector**

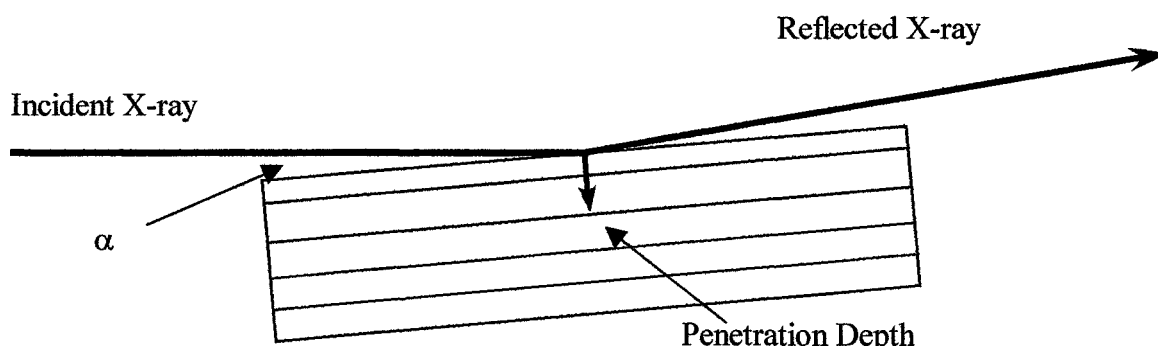
The GIXRD method also takes out the substrate from the scan. As in the powder method the substrate plays a huge part in the data that is collected. Figure 3.4 shows the fixed angle  $\alpha$  that the sample is kept at in relation to the incident x-ray beam. As the x-rays hit the sample they only penetrate so far into the film due to the grazing fixed angle. Most of the diffracted X-rays originate from the surface of the sample. For this reason this technique is very suitable for the analysis of thin films. The conditions for Bragg reflection is the same as for powder diffraction experiments, so you are able to predict where the diffraction peak will be for a certain material by using Bragg's equation.

Figure 3.4 also show a vector that is coming out of the sample or perpendicular to the crystalline plane. This is the scattering vector of the x-ray. In the powder method the scattering vector stay oriented in the same direction as shown in Fig. 3.3. The reason it stays constant is that the incident angle is moving and the detector is moving a double the

incident angle. In the GIXRD method the incident angle is kept constant so this means that the detector and the scattering vector are moving. The crystalline plane that causes the diffraction is randomly oriented in the film. So when the detector is scanning on the  $2\theta$  and the x-rays hit the crystalline plane it comes in at  $\theta$  and then diffracts at  $2\theta$  so the detector picks up the diffraction peak. The only diffracted peaks that are picked up are from the thin film or the silicon wafer or any other substrate that is being used. The information that GIXRD is providing is similar to the information provided by a powder diffraction experiment. It can tell you what type of material is present, what crystal structures are present, GIXRD does not work very well on thin films that are single crystalline. The GIXRD technique is only good to use if you have a polycrystalline material. So if you would measure a blank silicon wafer with this method you would not see anything do to that the wafer is cut from a single crystal. Even though it has its limitations it is still a very useful technique to use. There might be some cases where if you scan your sample with the powder technique your resolution it not that great. You might be having trouble resolving some peaks due to the high intensity silicon peaks. This is a good situation where you can use GIXRD to cut out the silicon peaks and just get the material peaks to identify the material and crystal structure. As I indicated the usefulness of GIXRD in the characterization of thin films and how it can complement the powder diffraction method. This still may not give all the answers that are wanted about the characteristic of the thin films being analyzed. There are cases that you might need some information on thickness and surface and interfacial roughness of a thin film.

## **X-RAY REFLECTOMETRY**

X-ray reflectometry (XRR) is a very powerful and non-destructive technique that can give you the information on film thickness, surface and interfacial roughness. With the Bede Scientific simulation software you can also estimate the density of the thin film layers. The Reflectivity is the ratio of reflected intensity to the incident intensity (Ref. #2 p.XX). X-rays have a refractive index in matter a little less than one. At grazing incidence, the x-ray is totally externally reflected from the surface of the sample. In this case there is a small penetration depth, and the specular reflected x-ray is then mainly dependent on the surface properties. In particular it senses the electron density near the surface (Ref #2, P. XX).



**Figure 11 Is a grazing incidence of the X-ray onto a sample and show the penetration Depth as a function of incident angle**

So when you look at the reflected intensity as a function of the angle of incidence you can get information about the film thickness, and surface and interfacial roughness. As the angle of incidences increase the penetration depth also increase into the film. The reflected intensity of the incident intensity also changes due to the penetration depth. There is one more factor that contributes to the change in the reflected intensity. This is the surface or near surface along with the interfacial roughness between the two different materials.

The X-ray reflectivity from a layered structure can be calculated by applying the recursive theory of Parratt (Ref #2, p.XX). The recursive theory of Parratt is a generalization of the Fresnel reflectivity theory of a system of flat; ideal layers each with a constant electron density. The refractive index  $n$  of a material can be given as:

$$n=1-\delta-i\beta \quad \text{Equation 3.5}$$

where  $\delta-i\beta$  can be written in terms of the sum of the atomic scattering factors of atoms of type (a). Which there is  $N_a$  in unit volume of the material:

$$\delta - i\beta = [(\lambda^2 r_e) / (2\pi)] \sum_a (Z_a + f'_a + if''_a) N_a \quad \text{Equation 3.6}$$

where  $Z_a$  is the atomic number of atomic species  $a$  and  $f'_a$ ,  $f''_a$  are the real and imaginary parts of the dispersion corrections to the atomic scattering factor of atomic species  $a$  (Ref #2, p.XX). This expression show that the refractive index of matter for x-rays is less than one. At glancing angles below the critical angle  $\theta_c$  the beam of x-rays are totally externally reflected from the surface. Applying Snell's law in the small angle approximation will give us an expression for the critical angle if the effects of absorption are neglected:

$$\theta_c = \sqrt{2\delta} \quad \text{Equation 3.7}$$

In the following section we will derive an equation for the reflectivity of a multilayer system. This is a system of  $N$  smooth, homogeneous layers (see Fig. 3.5) Assume refractive index of the  $j$ th layer is given by

$$n_j = 1 - \delta_j - i\beta_j \quad \text{Equation 3.8}$$

and the reflection amplitude of the interface between the  $j^{\text{th}}$  and the  $j-1^{\text{th}}$  layers can be denoted by  $r_{j-1,j}$ . The electric vector of the incident and reflected waves at the interface between the  $j^{\text{th}}$  and the  $j-1^{\text{th}}$  layers are denoted by  $E_{j-1,j}$ ,  $E_{j-1,j}^r$  respectively (Ref #2, p XX).

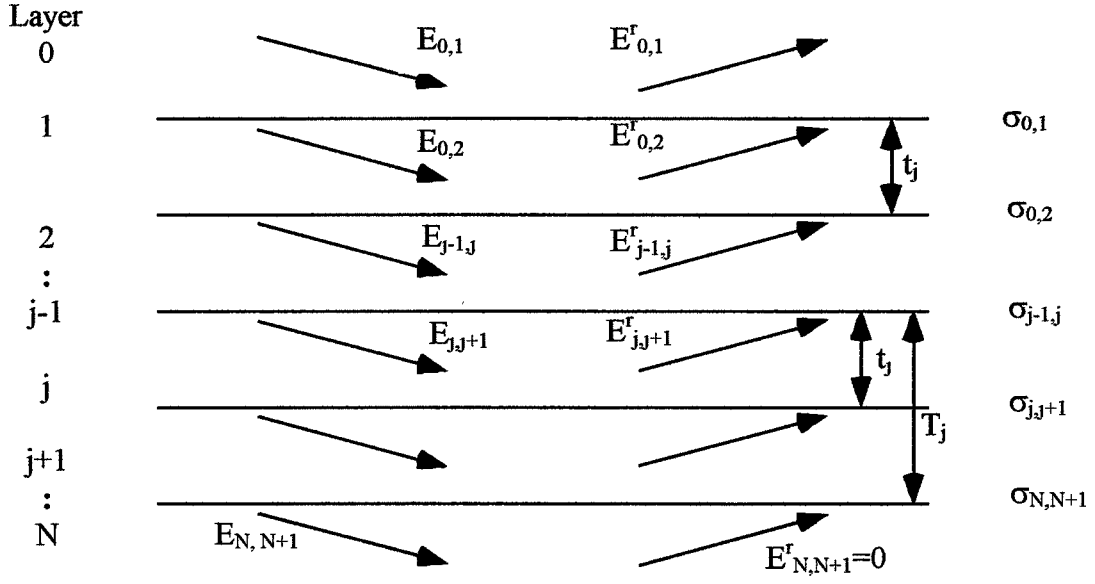


**Figure 12 The specular reflection of x-rays in a layered structure**

The tangential component of the electric field must be continuous at each of the  $j$  interfaces due to Maxwell's equations. Then the solution of this problem leads to a recursive formula of the reflection amplitude  $R_{j-1,j}$  of the stack layers from the substrate to the interface between the  $j^{\text{th}}$  and  $j-1^{\text{th}}$  layers (Ref #2, p. XX):

$$R_{j-1,j} = a_{j-1}^4 [(R_{j,j+1} + r_{j-1,j}) / (R_{j,j+1} r_{j-1,j} + 1)] \quad \text{Equation 3.9}$$

where

$$R_{j,j+1} = a_j^2 (E_{j,j+1}^r / E_{j,j+1}) \quad \text{Equation 3.10}$$

$$r_{j-1,j} = (f_{j-1} - f_j) / (f_{j-1} + f_j) \quad \text{Equation 3.11}$$

$$f_j = (\theta^2 - 2\delta_j - 2i\beta_j)^{1/2} \quad \text{Equation 3.12}$$

and  $a_j$  is the phase factor for half the thickness  $t_j$

$$a_j = \exp(-i(\pi/\lambda) f_j t_j) \quad \text{Equation 3.13}$$

Above equations can be used to find the reflectivity of the mulilayer. You have to start at a substrate and assume its thickness is infinite. Assume for the substrate that  $R_{N, N+1}$  is equal to zero. By solving the equation with  $j=N$  and by continuing recursively until the top layer is reached ( $j=1$ ) the reflectivity of the multilayers can be found:

$$R_{0,1} = E_{0,1}^r / E_{0,1} \quad \text{Equation 3.14}$$

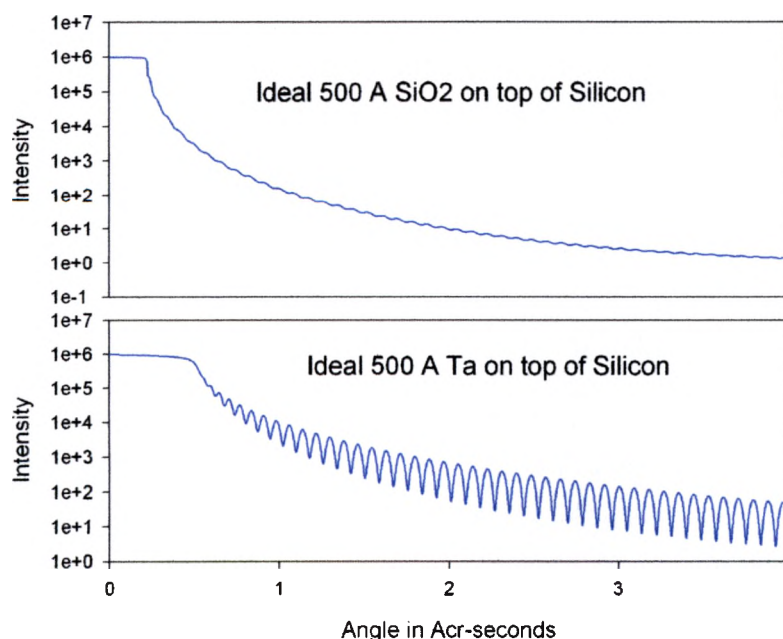
From this the ratio of the reflected to incident x-ray intensities is given by the product of  $R_{0,1}$  with its complex conjugate

$$I_r/I_o = |R_{0,1}|^2 \quad \text{Equation 3.15}$$

It is not easy to intepret X-ray Reflectivity (XRR) data via hand calculation. Bede Scientific has made it very simple to get the film thickness, surface and interfacial roughness using a powerful computer algorithm. Bede's REFS Mercury software is used to simulate XRR data. This program uses numerical integration of the Takagi-Taupin equation. This is a generalized form of the dynamical theory, to calculate the diffracted intensity (Ref #12, p. XX). This software is propriety of Bede Scientific so I do not have all the details of the actual fitting calculation that is used to obtain a "best" fit of the

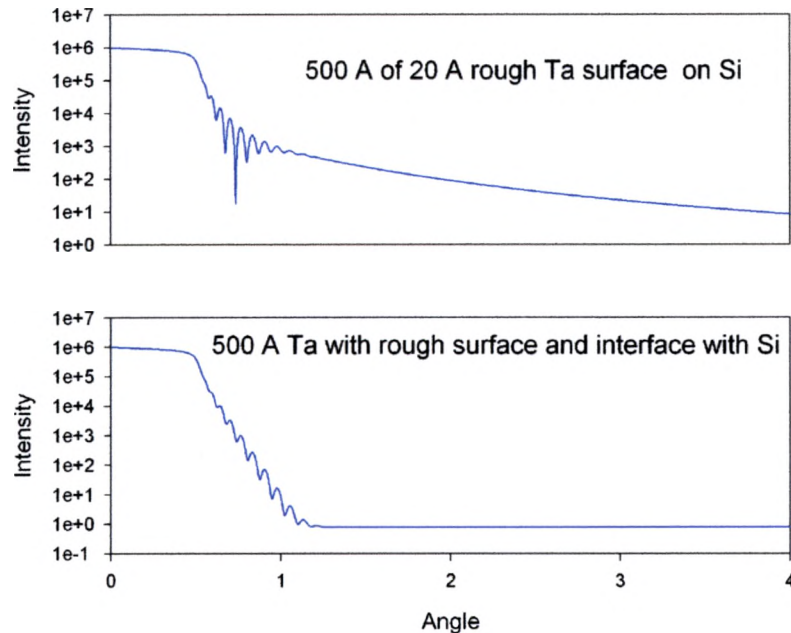
actual data using the general procedures I describe earlier. Though the software is very useful in finding the information that is needed. To simulate the XRR data certain properties for your system need to be known, for example the relative thickness of each layer and the type of material for each layer should be all that is needed to simulate the XRR data. From this point all you need to do is start the calculation and just wait until the fit is relatively close to the actual data.

Figure 3.6 is two simulations of two thin films on silicon. The thin films that I used in the two simulations are  $\text{SiO}_2$  and Ta. I simulated them as being the ideal layers with no roughness on top and at the interface between the Si and the Ta or the Si and the  $\text{SiO}_2$ . You can see the difference between the XRR simulations even though these films have the same thickness. You can see the sharp contrast between both simulations. The Si/ $\text{SiO}_2$  film has a sharp drop in intensity after the critical angle. The Si/Ta film has a gradual drop and you can see the periodicity of the x-ray intensity.



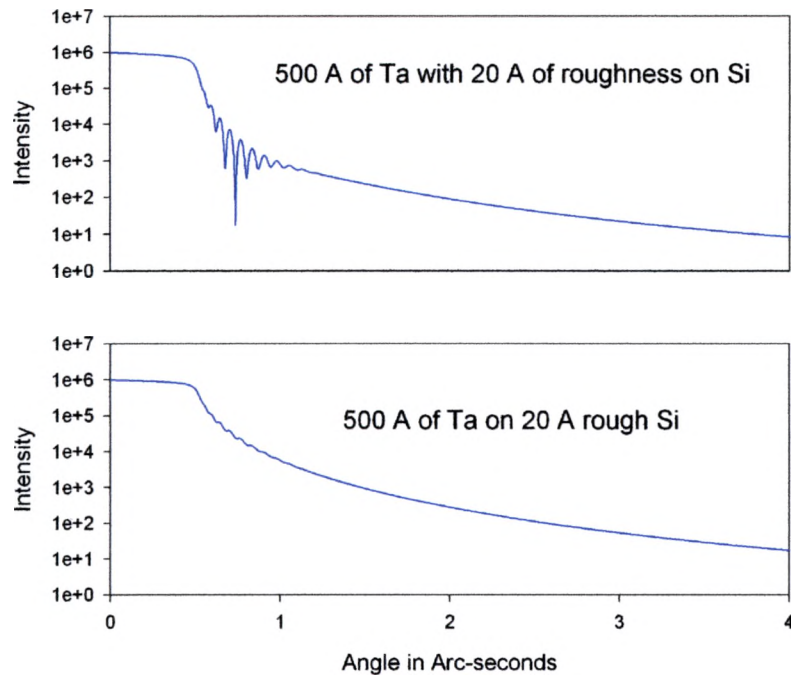
**Figure 13 Simulations of a 500 A  $\text{SiO}_2/\text{Si}$  and  $\text{Ta}/\text{Si}$**

In this set of simulations we have a Ta/Si layer with 20 Å rough top surface. The other simulation is of a Ta/Si layer where the Si has a 20 Å roughness. From this you can tell how much change occurs just by changing the roughness location.



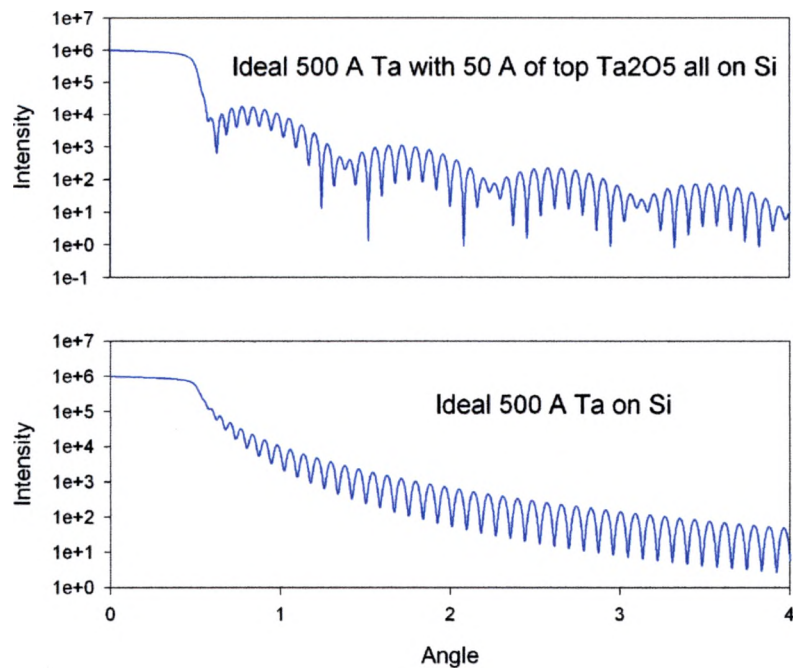
**Figure 14 500 Å Ta/Si film with 20 Å at interface Si/Ta and on Ta/air surface**

In this set of simulations you have the ideal 500 Å Ta/Si that was described earlier and we have an ideal 500 Å Ta on top of 50 Å Ta<sub>2</sub>O<sub>5</sub> on Silicon. From the simulation you can see the differences in the simulations. In the film with the Ta<sub>2</sub>O<sub>5</sub> has a second periodicity along with the similar periodicity as the ideal Ta/Si layer film.



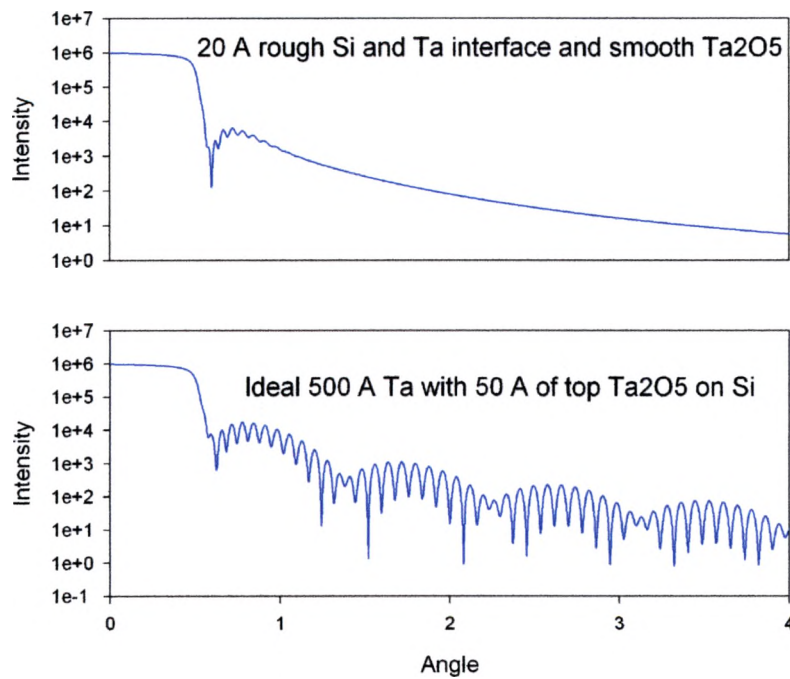
**Figure 15 Simulation of 500 Å Ta/Si with 20 Å roughness on Si compared with roughness on Ta**

Now the next Fig. 3.10 has two simulations, one being of the ideal 500 Å Ta/50 Å Ta<sub>2</sub>O<sub>5</sub>/Si and the other is the same but has a 20 Å rough Si and Ta interface with a smooth Ta<sub>2</sub>O<sub>5</sub>. This shows that the roughness completely changes the reflectivity curve depending where the roughness is located.



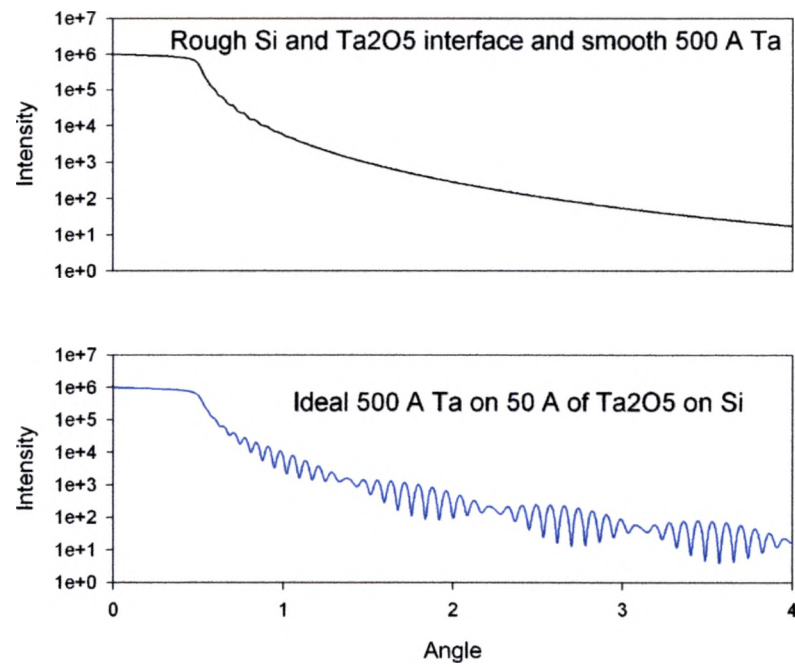
**Figure 16 Simluation of Ideal 500 Å Ta/Si compared with 500 Å Ta/50 Å Ta<sub>2</sub>O<sub>5</sub>/Si**

Figure 3.11 show what happens when you change the location of the roughness in the Ta/Ta<sub>2</sub>O<sub>5</sub>/Si film. The simulation shows that with a rough Si and Ta<sub>2</sub>O<sub>5</sub> interface destroys the periodicity of the film compared to the ideal simulation of the same film.



**Figure 17 Simulation of 20 Å rough Si and Ta with ideal Ta<sub>2</sub>O<sub>5</sub> compared with Ideal 500 Å Ta/50 Å Ta<sub>2</sub>O<sub>5</sub>/Si**

The last Fig 3.12 show how two different films can have very similar XRR curves. I compared a 500 Å Ti film on Silicon and a 400 Å Ti on a 100 Å TiN layer on silicon shows that they are very identical. There is very little change in x-ray reflectivity curve.



**Figure 18 Simulation of rough Si/Ta<sub>2</sub>O<sub>5</sub> interface with ideal Ta compared to Ideal 500 A Ta/50 A Ta<sub>2</sub>O<sub>5</sub>/Si**

By using this knowledge on XRR you can get a good understanding on how the simulations works to fit the actual data.

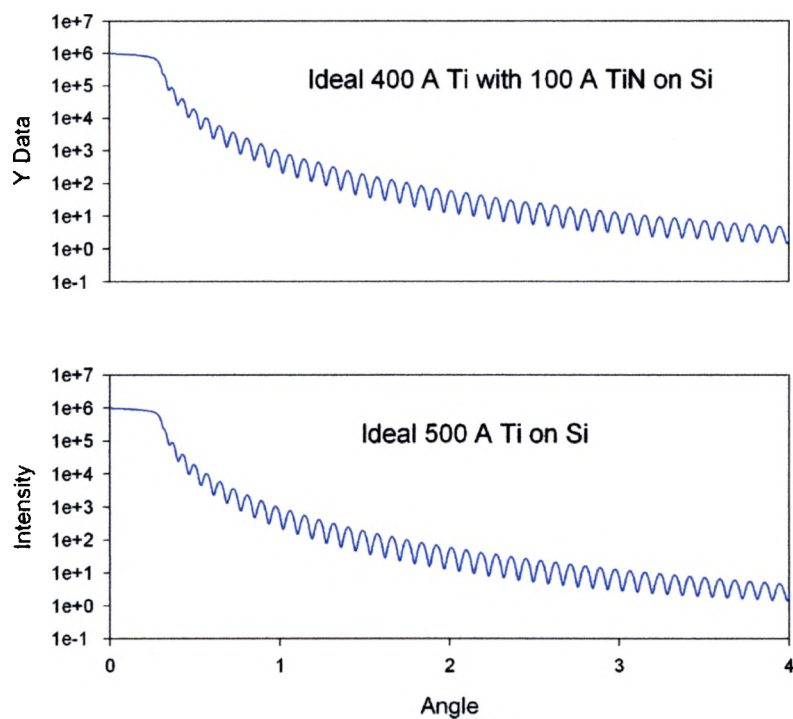


**Figure 19 Simulation of and Ideal 500A Ti/Si compared with Ideal 400 A Ti/100 A TiN/ Si**

## CHAPTER 4

### X-RAY DATA & RESULTS

This chapter presents x-ray analysis data I collected on the test films mention in earlier chapters. Most of this data was collected on the Bede D3 system at AMD, with additional data collected from the Bede 200 system at SWT. Generally, three different types of measurements were taken on the most of the samples: Powder X-ray Diffraction, Grazing Incidences X-ray Diffraction (GIXRD), and X-ray Reflectivity (XRR).

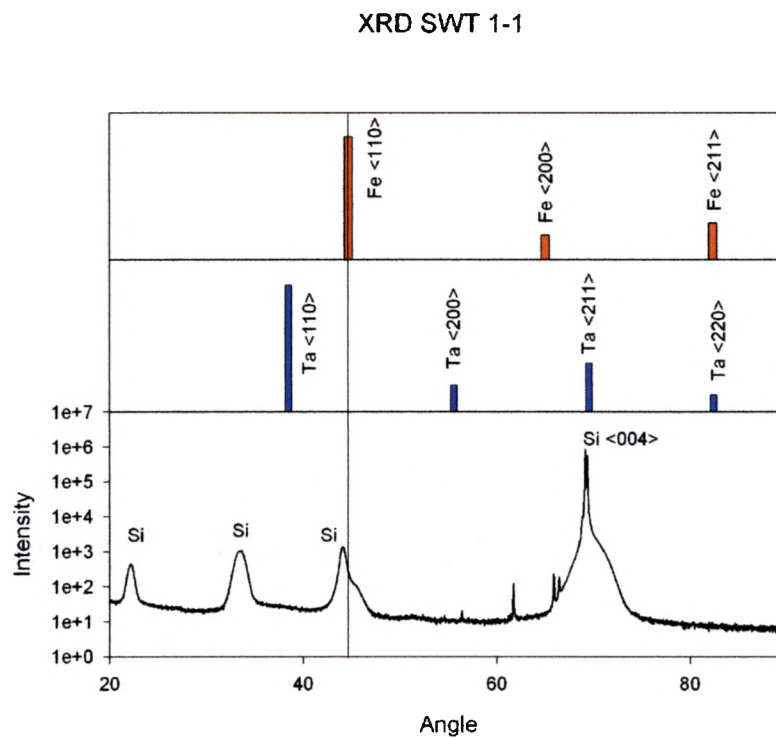
For Powder Diffraction the diffractometer was set to run at a  $\theta/2\theta$  (theta/2 theta) relation. The detector was link to run at  $2\theta$  while the Axis 2 (sample Axis) was moving at  $\theta$ . Most of the samples were grown on Silicon so I would first setup on silicon's strongest peak, which is at  $69.1^\circ$  ( $2\theta$ ). I aligned on this peak to make sure that the Detector and Axis 2 are truly following Bragg's relation. The data collection time varies on how long you want the detector to count before it moves to the next point. I usually have the D3 set with a 70-degree range that starts at 20 degrees and runs to 90 degrees. A typical scan takes approximately an hour or so.

The next set of data that I collected was the GIXRD. With this technique you are able to eliminate the strong silicon peak that comes out of the powder diffraction. As I discussed in the previous chapter this technique also follows Bragg's relation. By keeping the incident angle small this eliminates the silicon peaks due to the shallow depth

penetration of the x-rays. To setup this measurement I would make sure that the sample is parallel to the x-ray beam. Once it was then I would set the Axis 2 (sample axis) to a fixed degree and then scan the detector over a  $2\theta$  range. The scan range is from 20 to 70 degrees and this measurement took roughly approximately an hour and a half to complete.

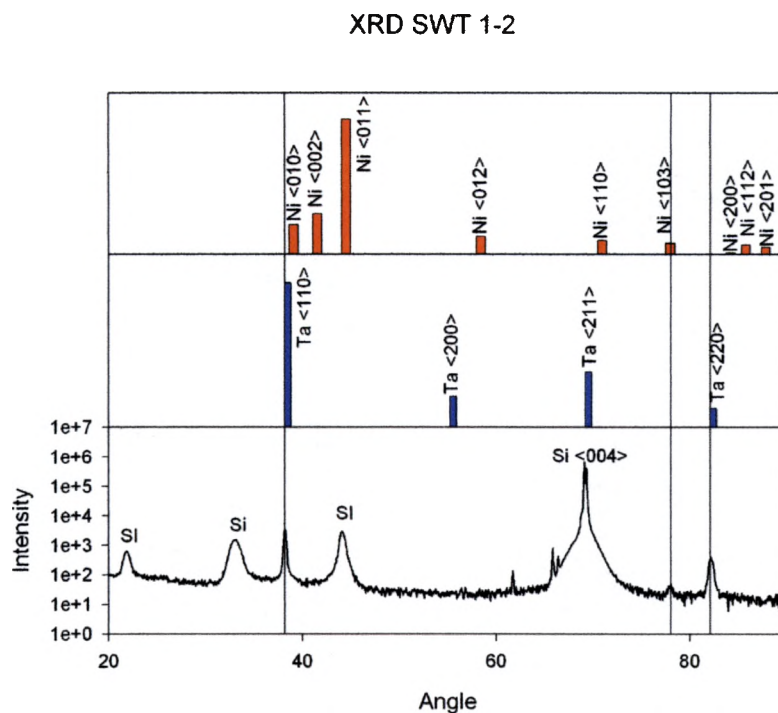
The last technique is XRR. This technique is a little more complicated to run. The reason it is more complicated is cause of the alignment that is needed to setup the scan. For both systems the Bede' 200 and the D3 use the same type of monochromator. The monochromators are specially manufactured silicon single crystals (channel cut collimators or CCC) that are specific cut along the  $\langle 220 \rangle$  plane. So when the Bede system is in the other two modes you would then need to align the channel cut crystals into place. By doing this you condition the beam in angle and also in wavelength. Once the desired wavelength is aligned then you are ready to start the measurement. The XRR measurement is also a grazing incidences and a  $\theta$  two  $\theta$ . This scan starts at 0 and ranges about 2 to 4 degrees. The zero start means that the sample is parallel and cuts the x-ray beam in half. I usually set the measurement to 7200 arc-seconds and take steps of a couple of arc-seconds to gather my data.

The first set of data is the Si/SiO<sub>2</sub>/NiFe/Ta/NiFe/Ta films that were fabricated by Robert Dail (MS Physics '96). This set of films was fabricated in the same manner. The basic recipe that was followed is Si wafer/1000Å of SiO<sub>2</sub>/10Å NiFe/100Å Ta/varying NiFe/ 100Å Ta.



**Figure 20 XRD scan of Si wafer/1000A SiO<sub>2</sub>/10A NiFe/100A Ta/300A NiFe/ 100A Ta.**

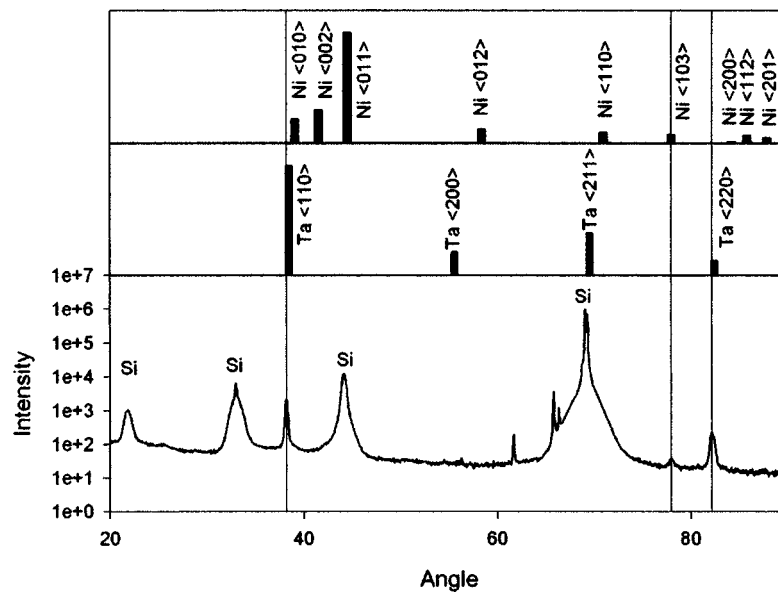
Figure 1 is the powder diffraction of SWT 1-1, which is Si wafer/1000A of SiO<sub>2</sub>/10A NiFe/100A Ta/300A NiFe/ 100A Ta. As you can see not much of the material that the model show is not present. For this data it is very hard to distinguish what material and crystalline phase is present.



**Figure 21 XRD scan of Si wafer/1000A SiO<sub>2</sub>/10A NiFe/100A Ta/300A NiFe/ 100A Ta**

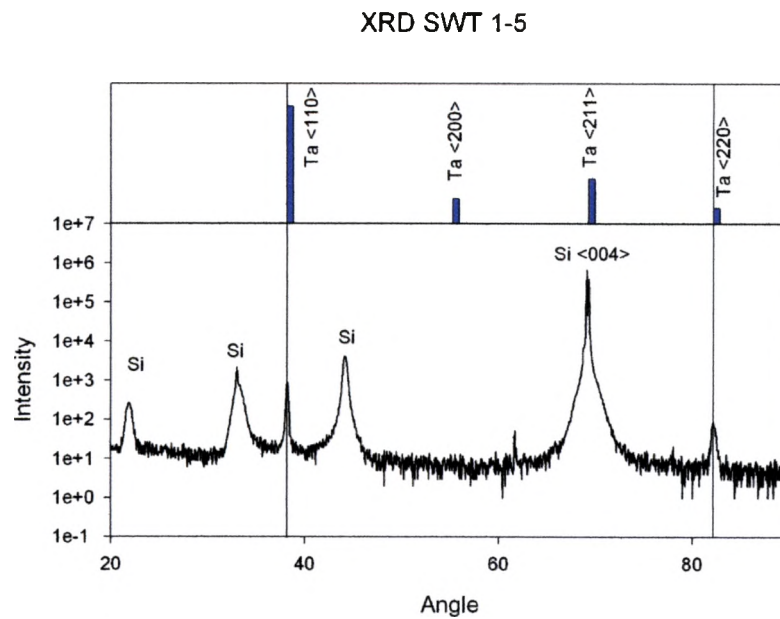
Figure 2 is the powder diffraction of Film SWT1-2, this is very similar to Fig. 1 except for this deposition they used the assist ion gun to help deposit the film. The Stack is still the same of Si wafer/1000A of SiO<sub>2</sub>/10A NiFe/100A Ta/300A NiFe/ 100A Ta. This data show very well that there is Ta present in this film. Which means that they were able to grow crystalline Ta by using the assist gun

## XRD SWT 1-4



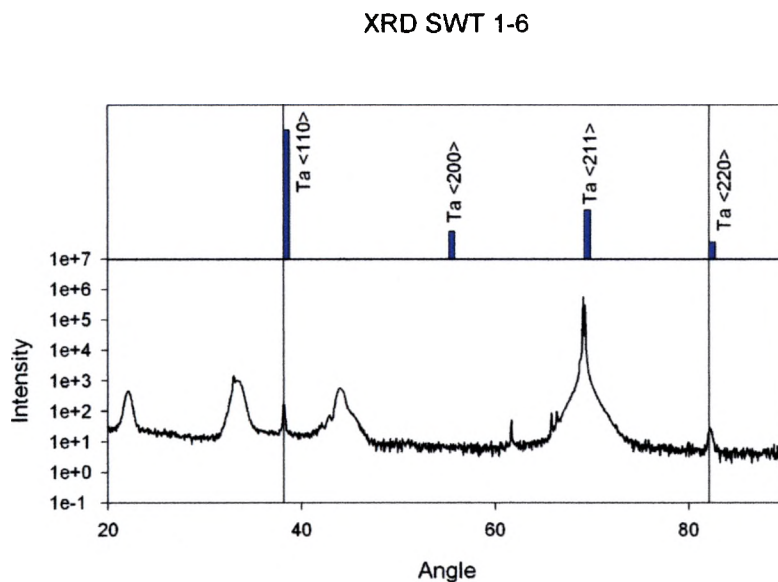
**Figure 22 XRD scan of Si wafer/1000A  $\text{SiO}_2$ /10A NiFe/100A Ta/500A NiFe/ 100A Ta**

Figure 3 is a little different than the first to figures. This stack is Si wafer/1000A  $\text{SiO}_2$ /10A NiFe/100A Ta/500A NiFe/ 100A Ta. This film has a thicker NiFe film but from the powder diffraction data you can see that the only material that can be resolved is the Ta layers.



**Figure 23 XRD scan of Si wafer/1000Å SiO<sub>2</sub>/10Å NiFe/100Å Ta/300Å NiFe/ 100Å Ta**

This film stack is Si wafer/1000Å SiO<sub>2</sub>/10Å NiFe/100Å Ta/300Å NiFe/ 100Å Ta. This is very similar to Figure 1, but they increased the power of the deposition gun during the NiFe layer



**Figure 24 XRD scan of Si wafer/1000A SiO<sub>2</sub>/10A NiFe/100A Ta/300A NiFe/ 100A Ta**

For this film they lowered the power of deposition gun to about 300 eV, 50 mA for the deposition of the 300A NiFe layer. This films stack is Si wafer/1000A SiO<sub>2</sub>/10A NiFe/100A Ta/300A NiFe/ 100A Ta. The data for this film shows that only the Ta layers can be resolved by this method.

## XRD SWT 1-7

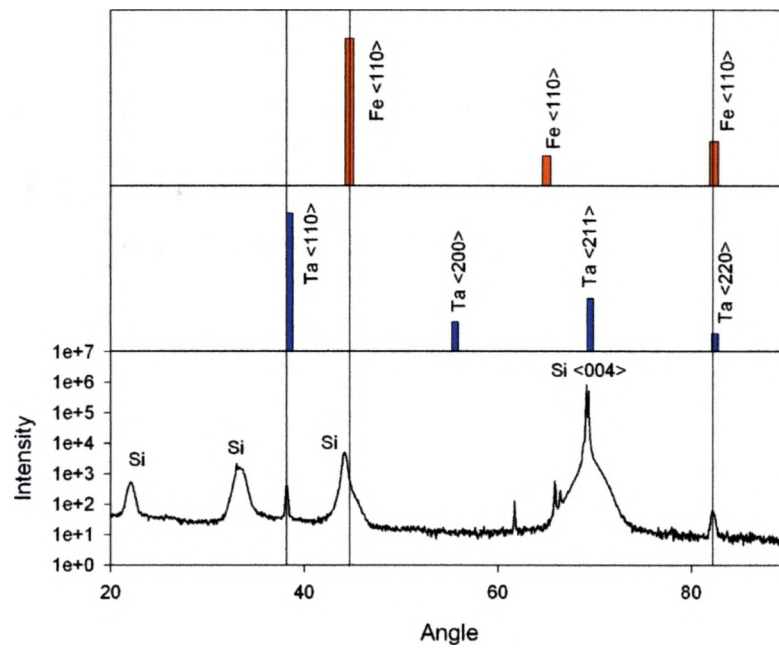


**Figure 25 XRD scan of Si wafer/1000A SiO<sub>2</sub>/10A NiFe/100A Ta/500A NiFe/ 100A Ta**

This sample is Si wafer/1000A SiO<sub>2</sub>/10A NiFe/100A Ta/500A NiFe/ 100A Ta. As you can see again that this film also has crystalline Ta present and we cannot see any other material from the stack.

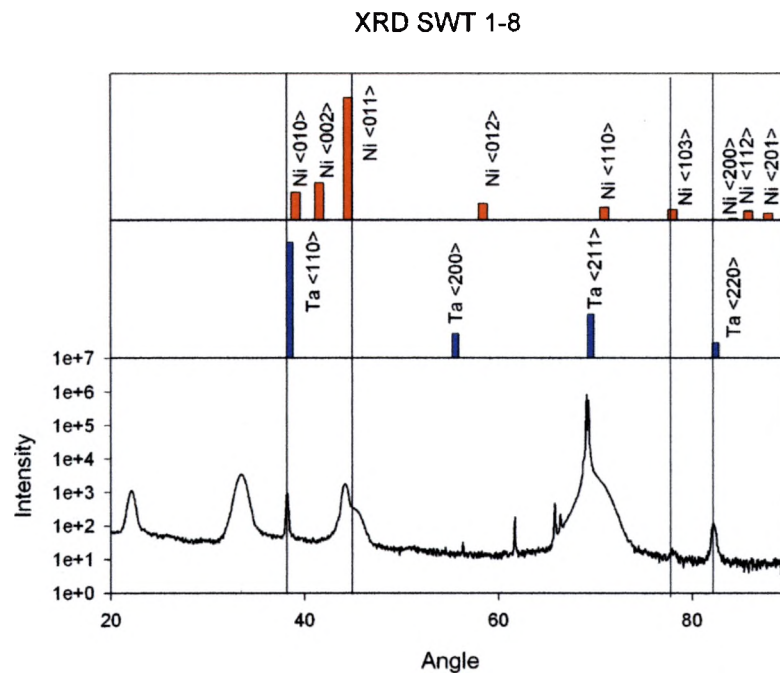


**Figure 26 XRD scan of Si wafer/1000A SiO<sub>2</sub>/10A NiFe/100A Ta/200A NiFe/ 100A Ta**

This last film has a thinner NiFe layer so the stack is Si wafer/1000A SiO<sub>2</sub>/10A NiFe/100A Ta/200A NiFe/ 100A Ta. We are still able to see the Ta in the data. Again this technique cannot resolve any other peaks that may be present.

Most of these films all have the same layering of a small seed layer of Permalloy with about 100 Angstroms of Tantalum with a varying layer of Permalloy and it is all capped with a 100 Angstroms of Tantalum. As you can see from this data of the SWT films it wasn't always clear what material was present. On certain films I saw the Tantalum versus any other of the material present. Then there were some cases where I didn't see anything to conclusive of what material was present. The samples I used were very small compared to the full 8-inch wafers I was used to at AMD. But I also have some more powder diffraction data that is obvious to what material is present. These

samples are from AMD and Lucent Technologies. My analysis indicates that these films are not single crystal or textured. This suggests that they are very randomly oriented.

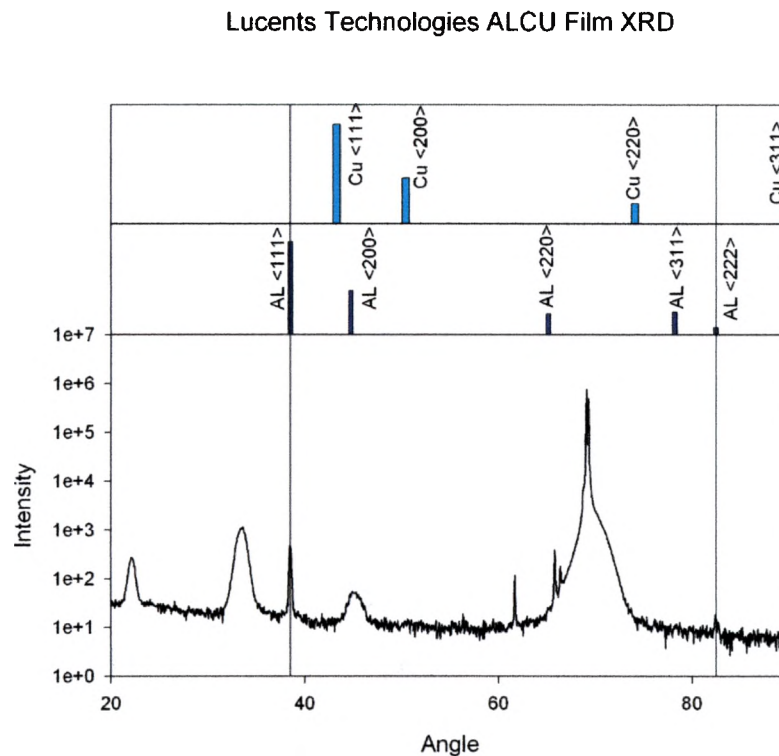


**Figure 27 XRD scan of Lucent Technologies 5000 Å AlCu film**

This film is a basic blanket film of Al that has a small percentage of Cu. As you can see the powder diffraction is able to pick up the Al peaks which also shows that this film is highly textured in the <111> crystalline phase.

### Lucent Technologies Ta/TaN Films

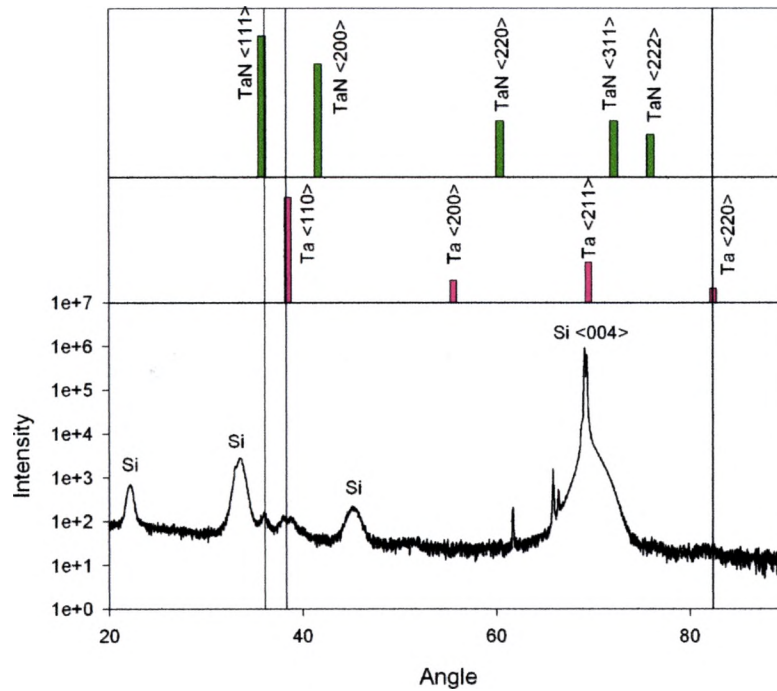


**Figure 28 XRD scan of Lucent Technologies 500 Å Ta/TaN film**

This film is also a blanket film but of Ta with some TaN on top. As this data shows that this film is also highly textured Ta & TaN film with the <110> crystalline phase.

## AMD Collimated Ti

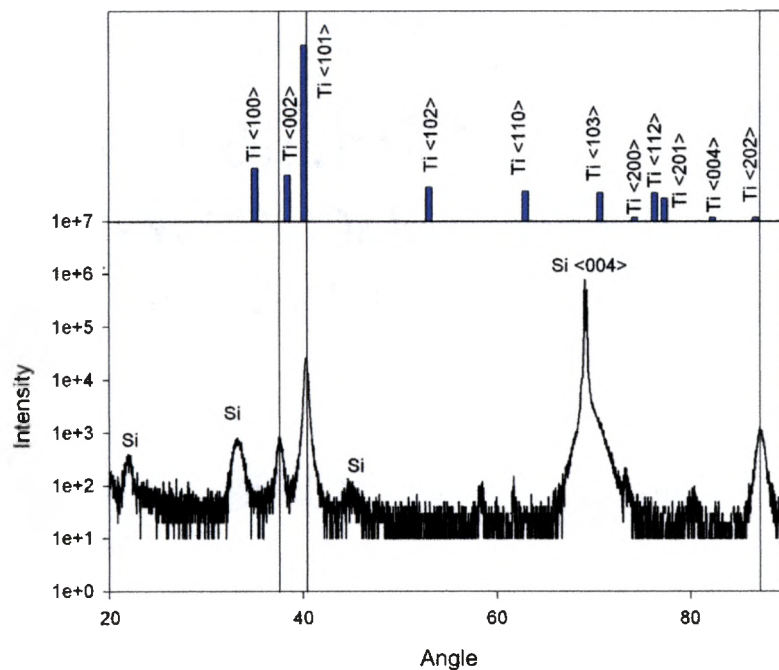


**Figure 29 XRD scan of AMD 300 A Ti film**

This film is a blanket film of Ti that was deposited by Collimated PVD system. The data shows that this film has two phase of Ti  $<101>$  and  $<002>$ .

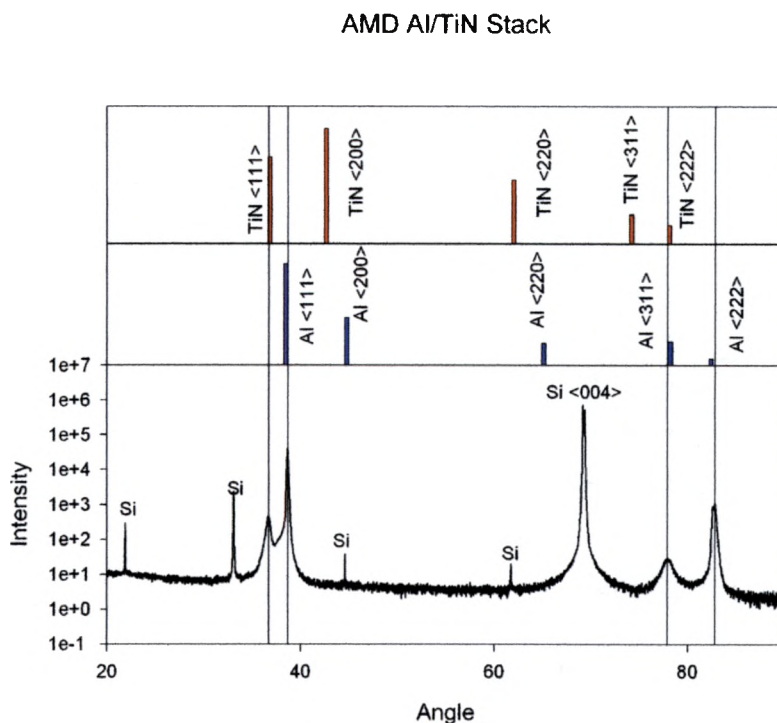


**Figure 30 XRD scan of AMD 5000 A Al/TiN stack film**

As you can see from this data that the elemental peaks are very distinct to each material.

As in the Lucent Technologies films you see that the Al peaks match closely to the powder diffraction data as well as the Tantalum and Tantalum Nitride peaks in Fig 9.

The first AMD film Fig. 10 shows clearly that Ti is present, and from this you see that there is two crystalline phases present in this film. They are the <002> and the <101> crystalline plane. The <202> plane is a multiple of the <101> plane. Figure 11 of the Al/TiN stack from AMD shows that this film is highly textured in the Al <111> and the TiN <111>. So as you can see from this set of data that in some cases it is hard to characterize the thin film, but in others it is very distinct on what the film is. So when you run into a problem like this you need to find another method that can characterize that material. So by using GIXRD is a very useful way of doing this.

This next set of data will be very similar to the previous set as far as the SWT films grown By Robert Dail (MS Physics '96). Then I'll show you some other data from AMD and Lucent Technologies.

GIXRD of a SWT 1-1 Film at 1 Degrees of Incidence

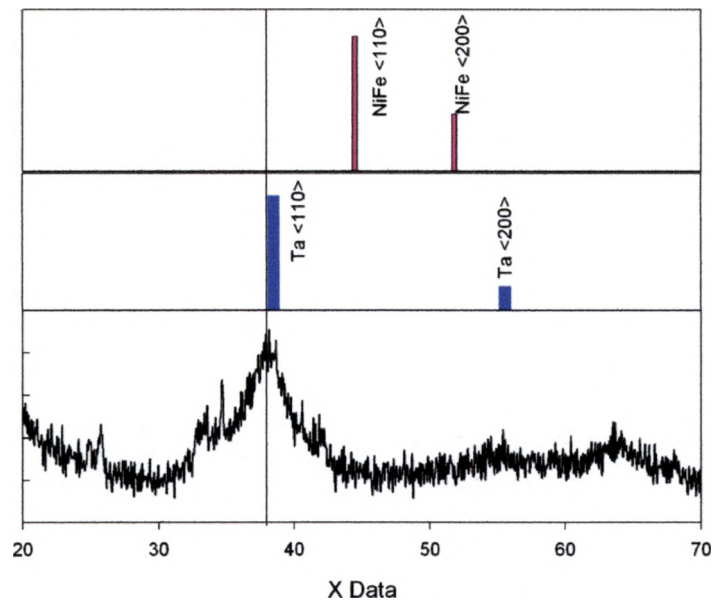


**Figure 31 GIXRD scan of Si wafer/1000A SiO<sub>2</sub>/10A NiFe/100A Ta/300A NiFe/ 100A Ta at 1 degree of incidences**

GIXRD of a SWT 1-1 Film at 1.5 Degrees of Incidence

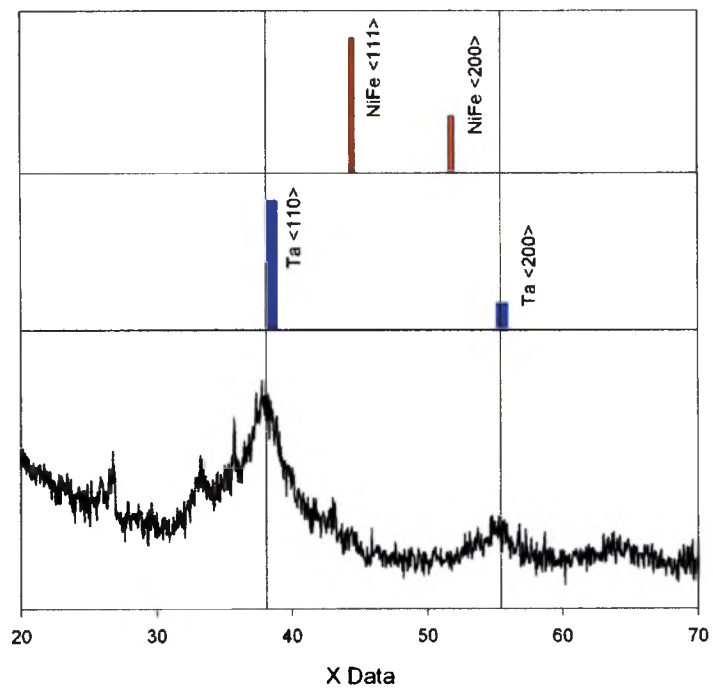


**Figure 32** GIXRD scan of Si wafer/1000Å SiO<sub>2</sub>/10Å NiFe/100Å Ta/300Å NiFe/ 100Å Ta at 1.5 degree of incidences

## GIXRD of a SWT 1-1 Film at 2 Degrees of Incidence

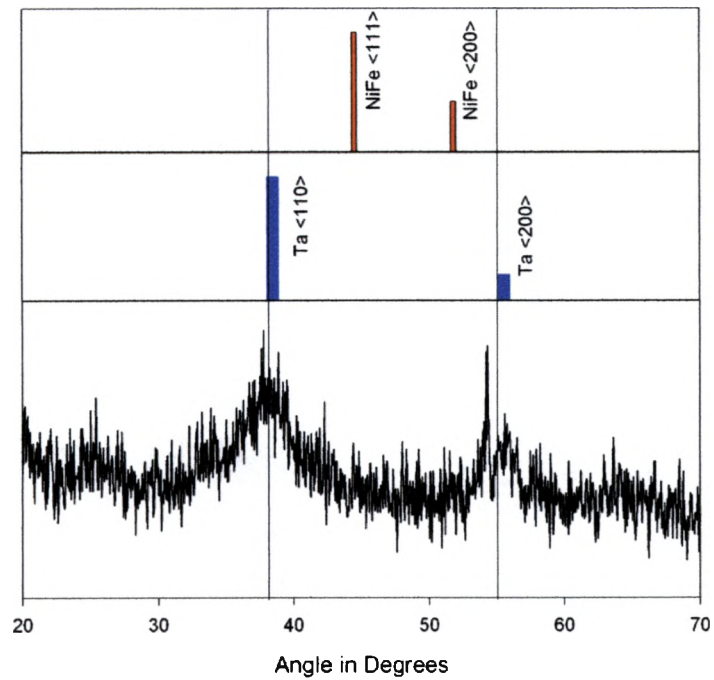


**Figure 33** GIXRD scan of Si wafer/1000Å SiO<sub>2</sub>/10Å NiFe/100Å Ta/300Å NiFe/ 100Å Ta at 2 degree of incidences

### GIXRD of a SWT 1-2 Film at 2 Degrees of Incidence

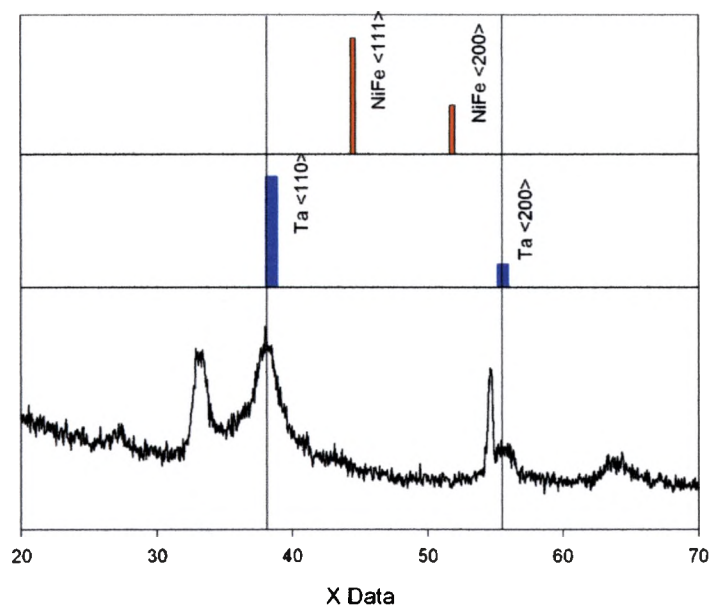


**Figure 34** GIXRD scan of Si wafer/1000Å SiO<sub>2</sub>/10Å NiFe/100Å Ta/300Å NiFe/ 100Å Ta at 2 degree of incidences

## GIXRD of a SWT 1-3 Film at 1 Degrees of Incidence

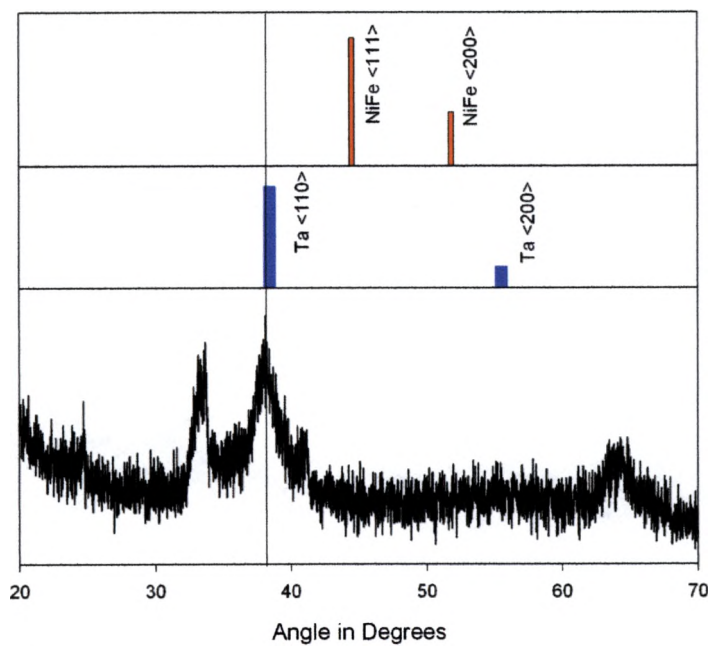


**Figure 35 GIXRD scan of Si wafer/1000Å SiO<sub>2</sub>/10Å NiFe/100Å Ta/200Å NiFe/ 100Å Ta at 1 degree of incidences**

## GIXRD of a SWT 1-3 Film at 2 Degrees of Incidence

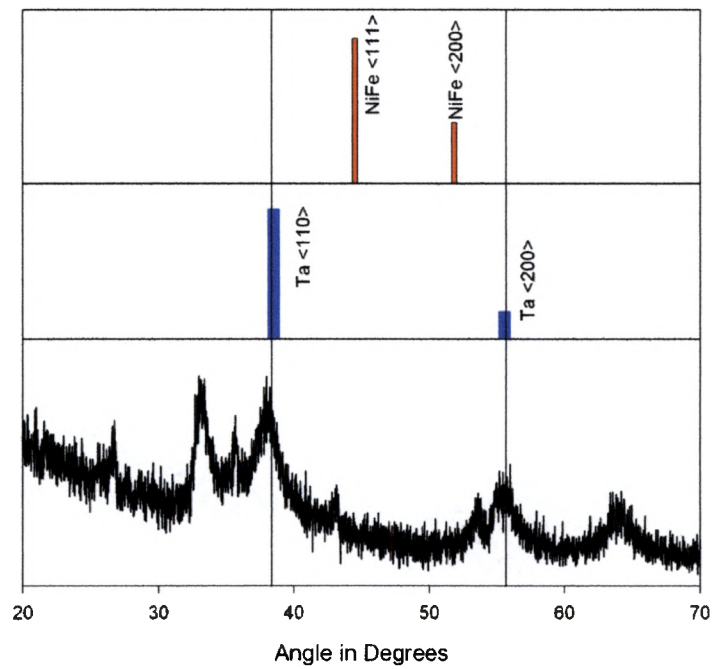


**Figure 36 GIXRD scan of Si wafer/1000Å SiO<sub>2</sub>/10Å NiFe/100Å Ta/200Å NiFe/ 100Å Ta at 2 degree of incidences**

## GIXRD of a SWT 1-4 Film at 1 Degrees of Incidence

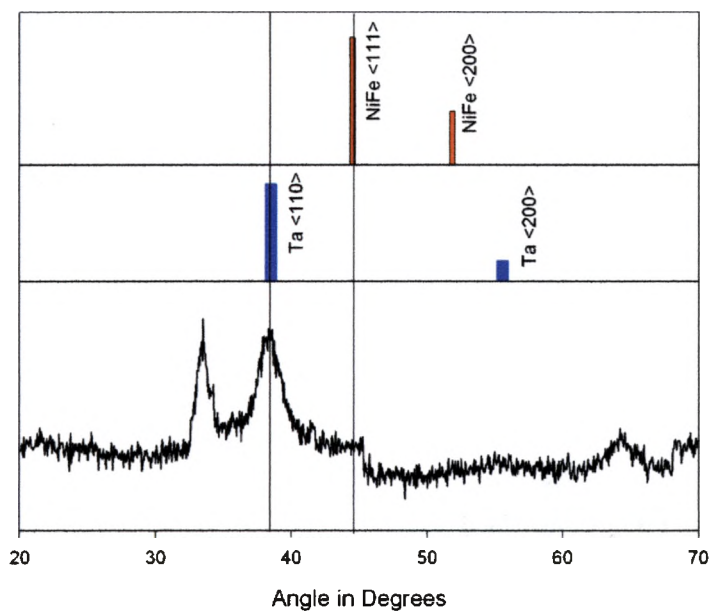


**Figure 37 GIXRD scan of Si wafer/1000A SiO<sub>2</sub>/10A NiFe/100A Ta/500A NiFe/ 100A Ta at 1 degree of incidences**

GIXRD of a SWT 1-4 Film at 2 Degrees of Incidence

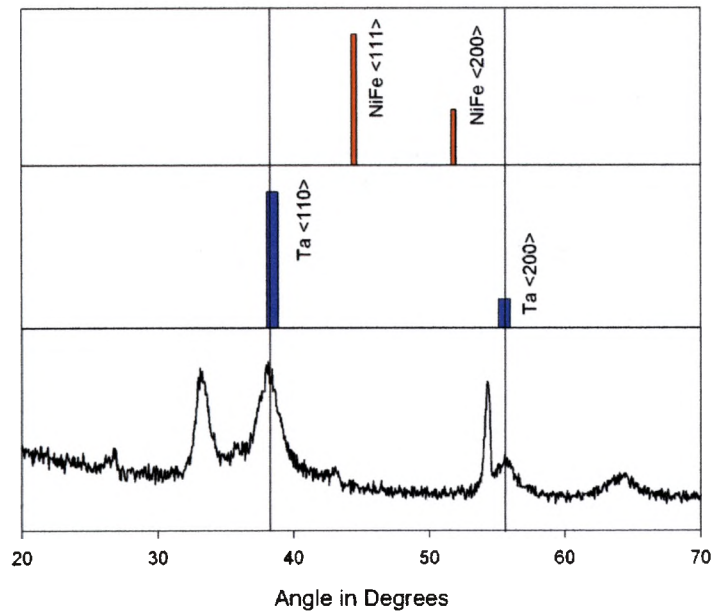


**Figure 38** GIXRD scan of Si wafer/1000A SiO<sub>2</sub>/10A NiFe/100A Ta/500A NiFe/ 100A Ta at 2 degree of incidences

GIXRD of a SWT 1-5 Film at 1 Degrees of Incidence

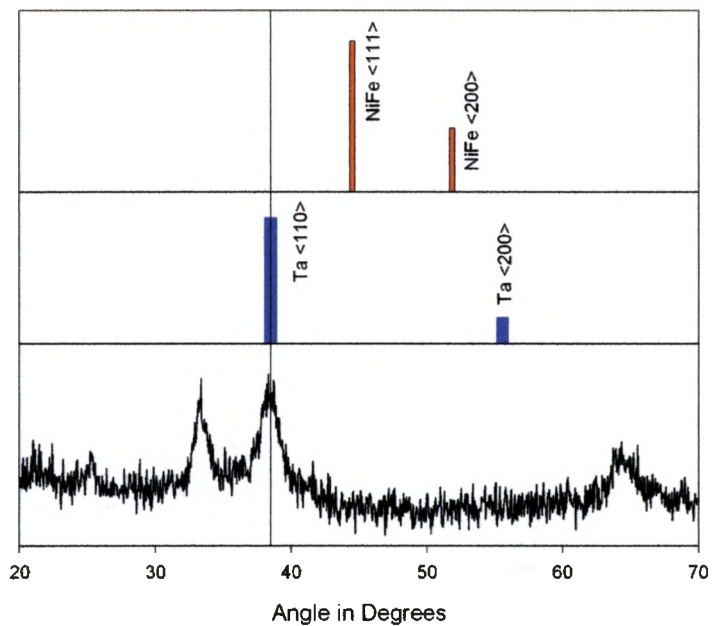


**Figure 39 GIXRD scan of Si wafer/1000A SiO<sub>2</sub>/10A NiFe/100A Ta/300A NiFe/ 100A Ta at 1 degree of incidences**

GIXRD of a SWT 1-5 Film at 1.5 Degrees of Incidence

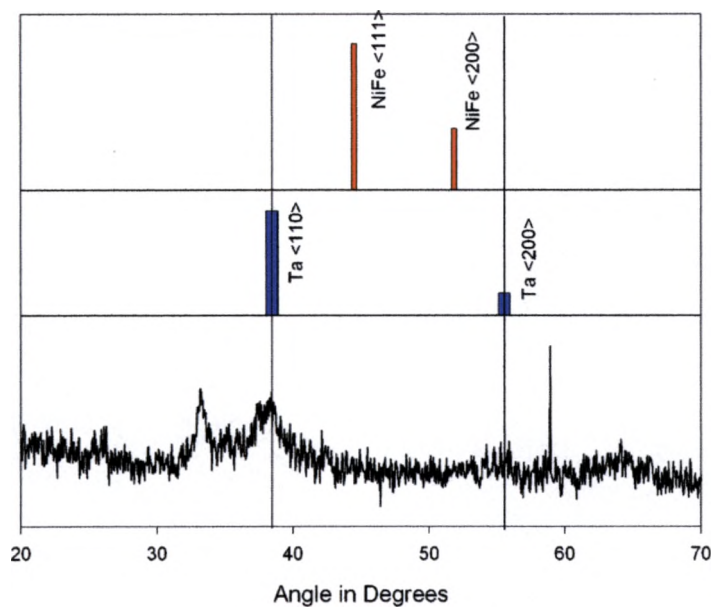


**Figure 40 GIXRD scan of Si wafer/1000A SiO<sub>2</sub>/10A NiFe/100A Ta/300A NiFe/ 100A Ta at 1.5 degree of incidences**

GIXRD of a SWT 1-5 Film at 2 Degrees of Incidence

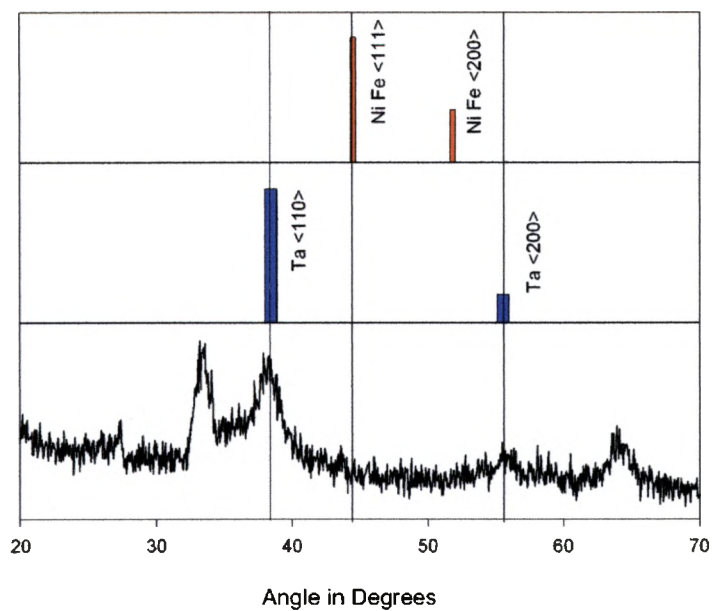


**Figure 41 GIXRD scan of Si wafer/1000A SiO<sub>2</sub>/10A NiFe/100A Ta/300A NiFe/ 100A Ta at 2 degree of incidences**

GIXRD of a SWT 1-6 Film at 2 Degrees of Incidence

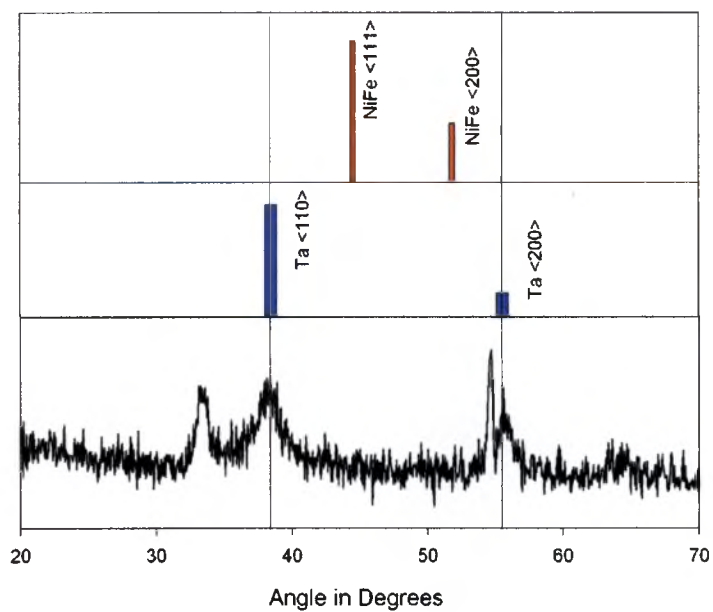


**Figure 42 GIXRD scan of Si wafer/1000A SiO<sub>2</sub>/10A NiFe/100A Ta/300A NiFe/ 100A Ta at 2 degree of incidences**

GIXRD of a SWT 1-8 Film at 2 Degrees of Incidence

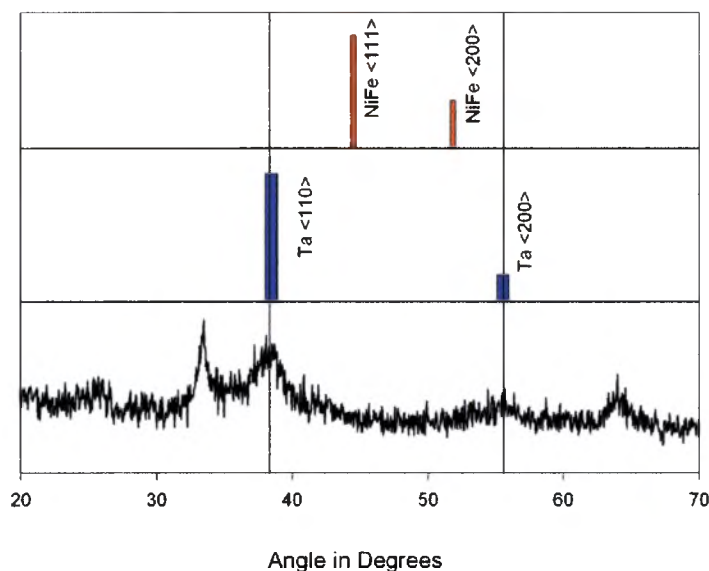


**Figure 43 GIXRD scan of Si wafer/1000Å SiO<sub>2</sub>/10Å NiFe/100Å Ta/300Å NiFe/ 100Å Ta at 2 degree of incidences**

In this data we are able to see that there is definitely Tantalum present in all of these films. There should also be some NiFe present in all of these films but only a few show some trace of NiFe. In couple of these films there are two peaks that I haven't been able to identify because for most of the materials used in making these films don't have any diffraction peaks where these two peaks or located. But, the differences between Powder and Grazing incidences are easy to see. The relative intensities of the Si Substrate are much lower in GIXRD versus Powder, which gives you a better resolution for thin films.

The next sets of films are from Lucent Technologies and a couple that Matt Langendorf will be using in his thesis. These are a lot more concrete on what type of material are present in each film.

AlCu film from Lucent Technology

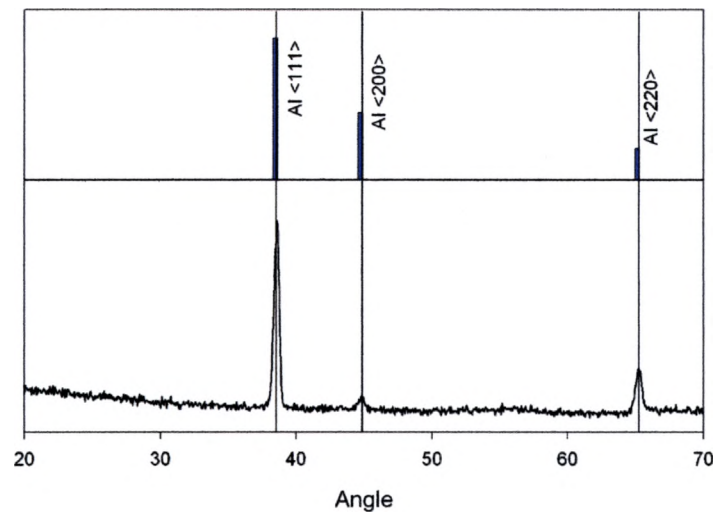


**Figure 44 GIXRD scan of Lucent Technologies 5000 Å AlCu film**

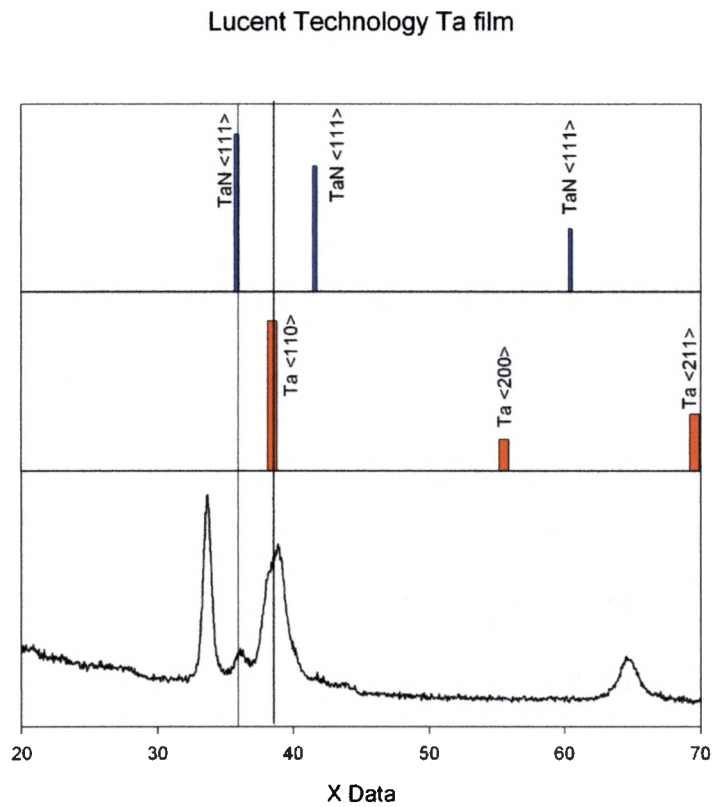


**Figure 45 GIXRD scan of Lucent Technologies 500 Å Ta/TaN film**

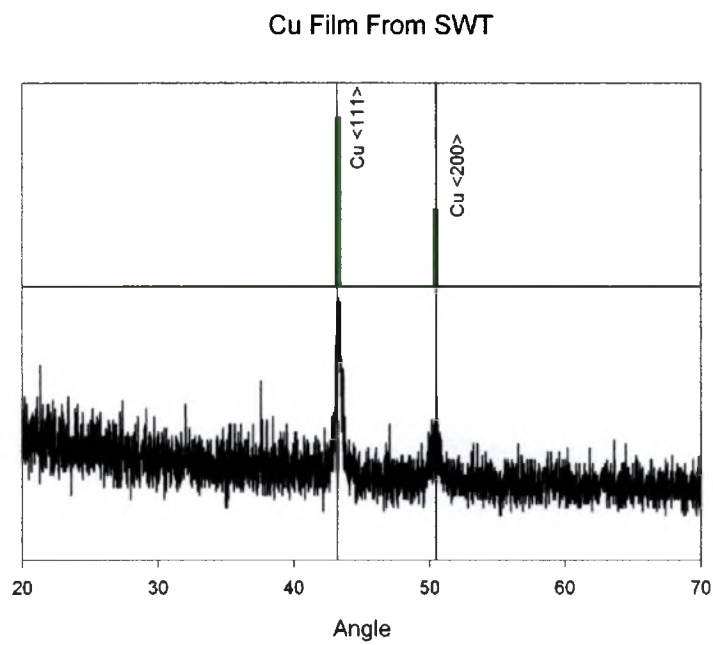


**Figure 46 1000Å Cu film**

In this set of Lucent Technologies film we can see that the Al in the film is very polycrystalline from the Fig. In the second you can see that Tantalum is present along with Tantalum nitride. In this sample there is mystery peaks that I have not found what they are. From the information that I received on these films is that the only material present should be Tantalum and Tantalum nitride. Note that in Fig. 27 the poor signal for such a thick film. This indicates that the XRD is not sensitive to Cu. This could also be the problem why we can see the Permalloy films. As you can see from looking at the powder data and GIXRD data that it is still not easy to analyze. So by using both techniques you can improve your results on making a definite match on what material and crystal structure is present in the thin film.

The last set of data is screen shots of Bede Scientific's REFS Mercury software that is used to simulate the Reflectivity data. Before you start looking at the data you need to know what everything in the shot is and means. I will follow this order in the shots for each film that I was able to analyze. The first shot is of the input tab. In the input tab you have a lot of parameters that you can change according to what material you are fitting. You can fit up to 9 layers on one film. So in the layer box you can enter how many layers you want for you fit. The next box is the points box; this gives the program how many data points are in your experimental data so the fit can match the data points. The Omega Start box tells the software where the experimental data started. The Lambda box is where you can enter the wavelength of the x-ray used in you reflectivity measurement, for my analysis, I used  $\text{Cu K}\alpha 1$  (1.54Å). As Omega start was for the starting position of the measurement the Omega finish box is the stopping point of the measurement. The incident intensity box is to let the software know at what intensity is

the incident beam of the XRR measurement. The background intensity is if there is any background other than the x-ray source you can have is subtracted by entering the value in this box. Once this is close to the experimental setup then you can start inputting the relative thickness, roughness, and density of each layer in your model that will be used to fit your actual data. Once you have completed this you then go to the Graph tab and input your experimental data into the software so you can fit this data. The Graph tab is the next shot you will see and it shows you your actual data and the model that you just enter in the input tab. Next to the model is the where the software will show you the results as it goes through the calculation to fit the model. Above the results it shows you how many evaluations the computer has gone through and it also give you the best cost and Standardized cost of the fit. So as you start the fit the program will give you an update on how the fit is going and as the standardized cost get closer to 0.1 give you an indication on how good the fit of your actual data is. So now lets look at some of the fits I was able to get for the SWT films made by Robert Dail (MS Physics '96).

The SWT sets of films were all grown on Silicon and the film stack is:  $\text{SiO}_2/\text{NiFe}/\text{Ta}/\text{NiFe}/\text{Ta}$ . In this stack there was only one varying layer and that was the last NiFe layer in the stack. As you can see from Fig #A show the actual model that I used to fit the XRR data for some of the samples. Fig #A is only specific to sample SWT 1-3 but the material layer is the same for all the samples I was able to fit. I used seven layers to fit this data and I was able to get a good fit. The extra layer is due to the Ta oxidizing over time. I was able to calculate how much Ta was consumed by the oxygen. I new that when they grew these films the two Tantalum layers were  $\sim 100$  Angstroms thick. So I first let the Software vary every layer to fit that data. When the fit was

complete and it looked like a good fit I saw that most of these films had a ~50 Angstroms layer of  $\text{Ta}_2\text{O}_5$  on top. From this I was able to find the ratio of the thickness of Ta over the Thickness of  $\text{Ta}_2\text{O}_5$ . I first looked for the weight per mol of both Ta and  $\text{Ta}_2\text{O}_5$ . The Ta is 180.948 g/mol and the  $\text{Ta}_2\text{O}_5$  is 441.893 g/mol. Then I divided the weight per mol by the Density of the bulk material to get the volume per mol which for Ta = 11.03  $\text{cm}^3/\text{mol}$  and for  $\text{Ta}_2\text{O}_5$  is 53.88  $\text{cm}^3/\text{mol}$ . Then by knowing the thickness of the oxide layer I can get a good estimate of how much of the Tantalum layer was consumed by the oxide growth. So in order to grow ~50 Angstroms of  $\text{Ta}_2\text{O}_5$  you would only need about ~10 Angstroms of Tantalum. So the top layer of Tantalum should be ~90 angstroms thick due to the formation of  $\text{Ta}_2\text{O}_5$ .

$$\text{Ta thickness} = 0.205 * \text{Ta}_2\text{O}_5 \text{ thickness} \quad \text{Equation 4 1}$$

So as you can see for the first sample SWT 1-3 I just let Mercury software run with it varying every layer. By doing this I was able to get a good fit that is shown in Fig. #B. Also in Fig. #B you can see what the calculated thickness, roughness and the density of each layer. I show this for all the samples I was able to run the XRR measurement. On Figures G and H you can see where I put some constraints in of the two Tantalum layer to see if this would give me a better fit.

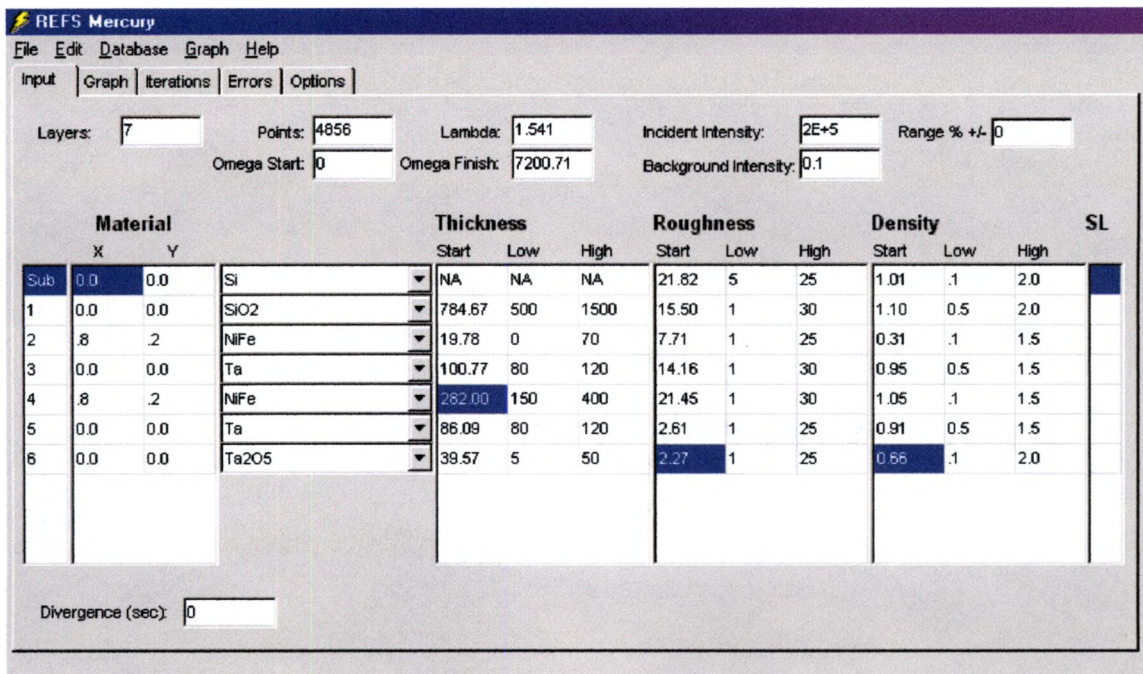


Figure 47 This is a screen shot of REFS Mercury Software Shows model that was used to fit sample SWT 1-3

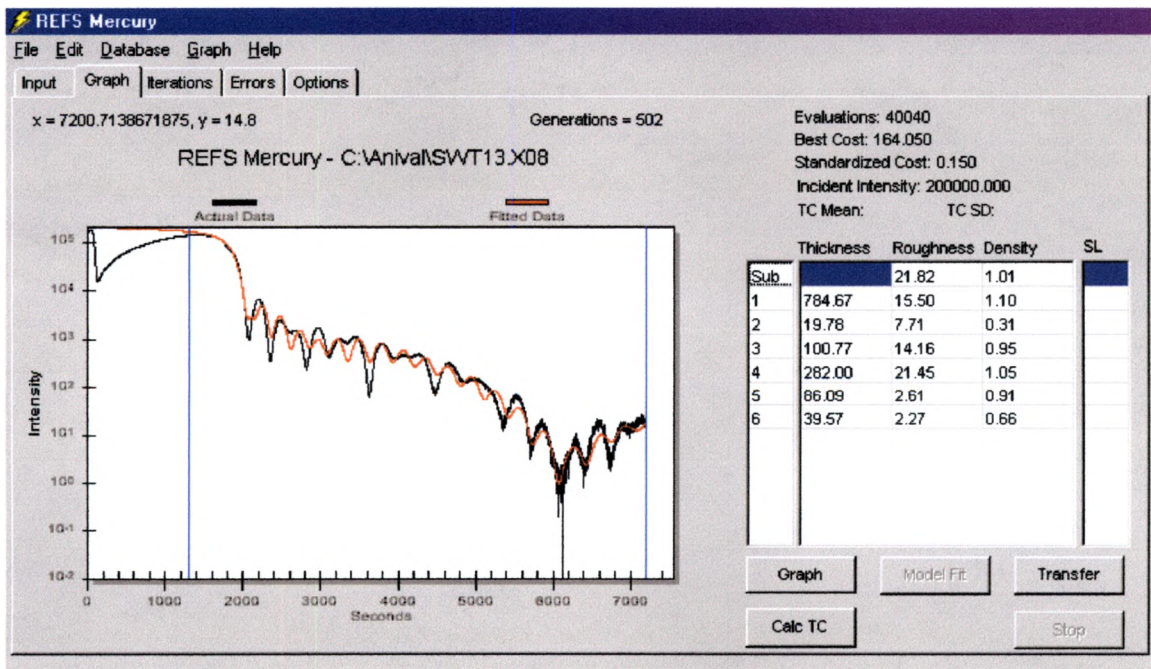


Figure 48 Screen Shot of REFS Mercury fitting the XRR data of SWT 1-3

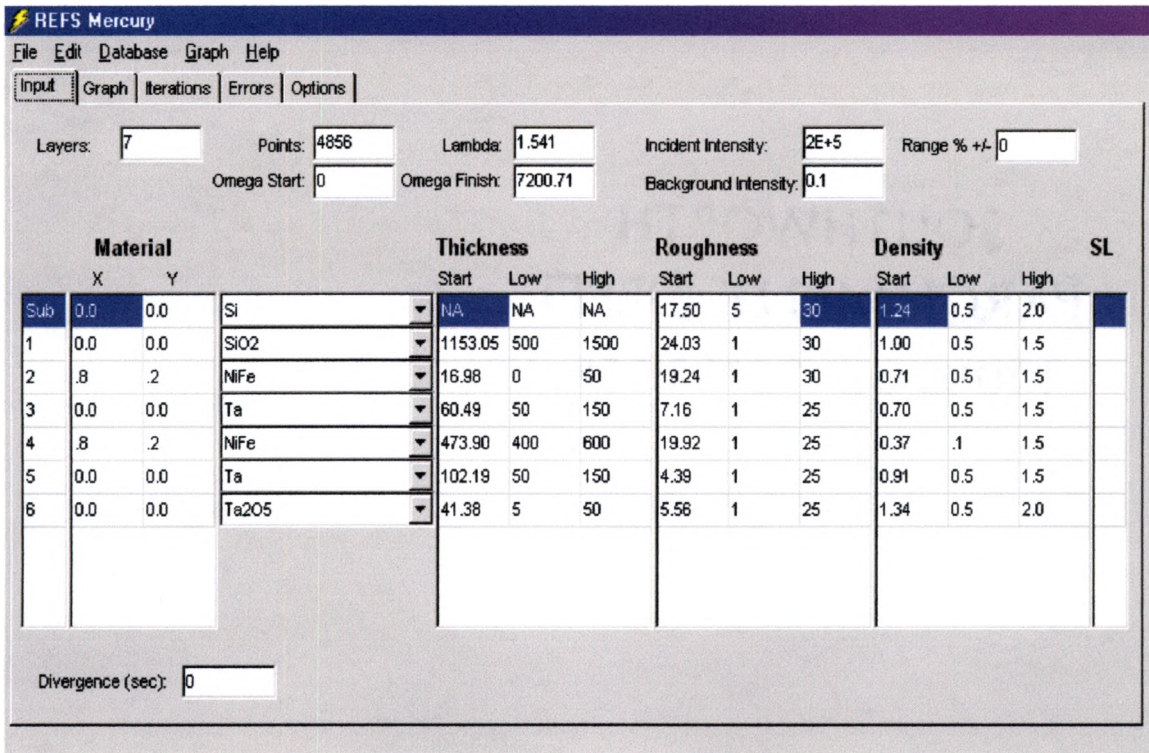


Figure 49 This is a screen shot of REFS Mercury Software Shows model that was used to fit sample SWT 1-4

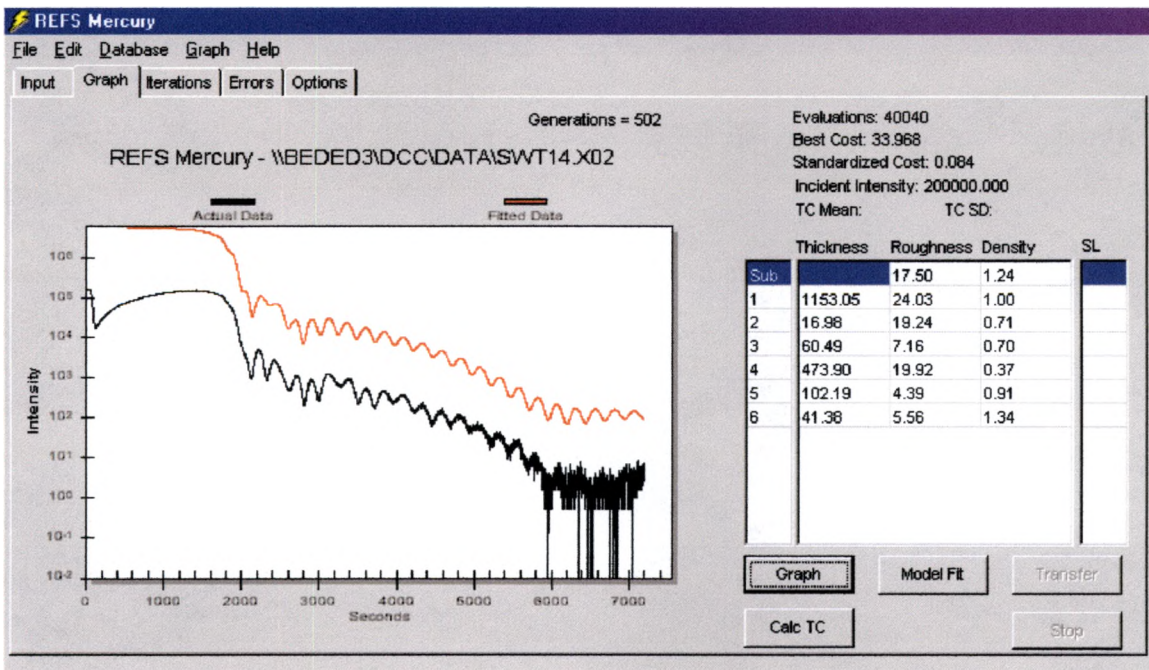


Figure 50 Screen Shot of REFS Mercury fitting the XRR data of SWT 1-4

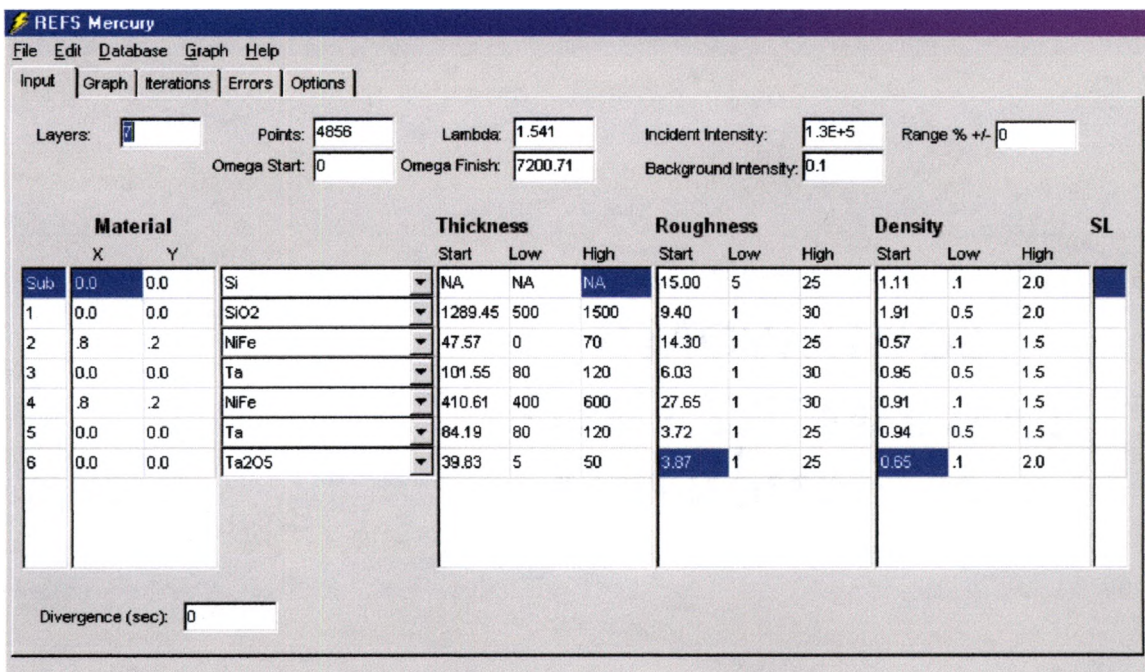


Figure 51 This is a screen shot of REFS Mercury Software Shows model that was used to fit sample SWT 1-5

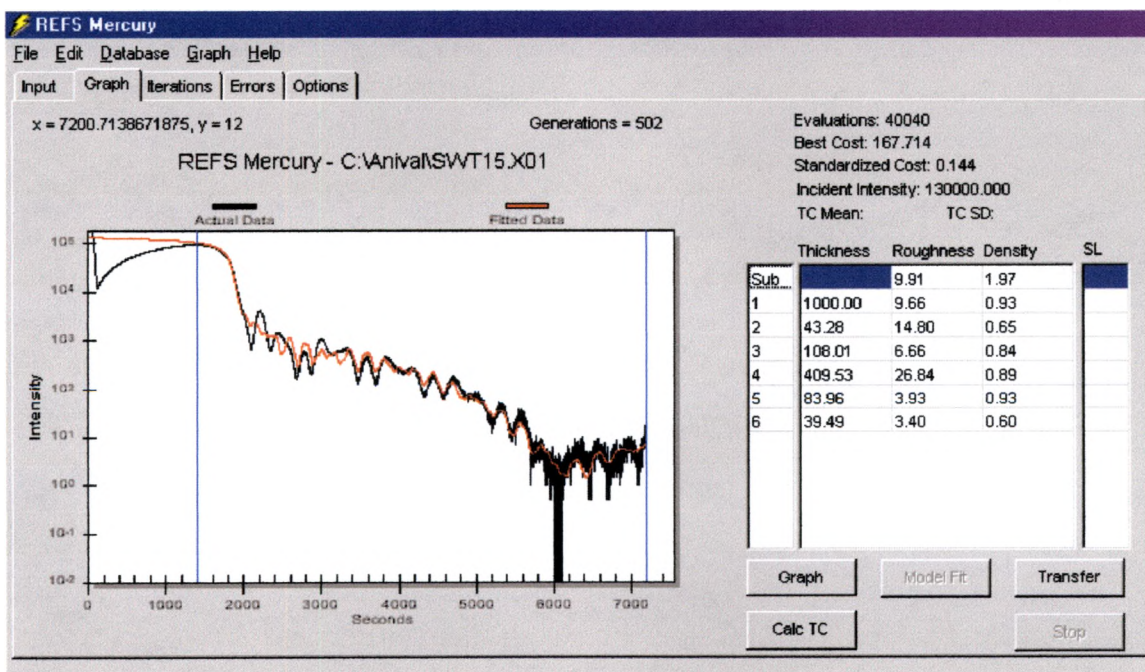


Figure 52 Screen Shot of REFS Mercury fitting the XRR data of SWT 1-5

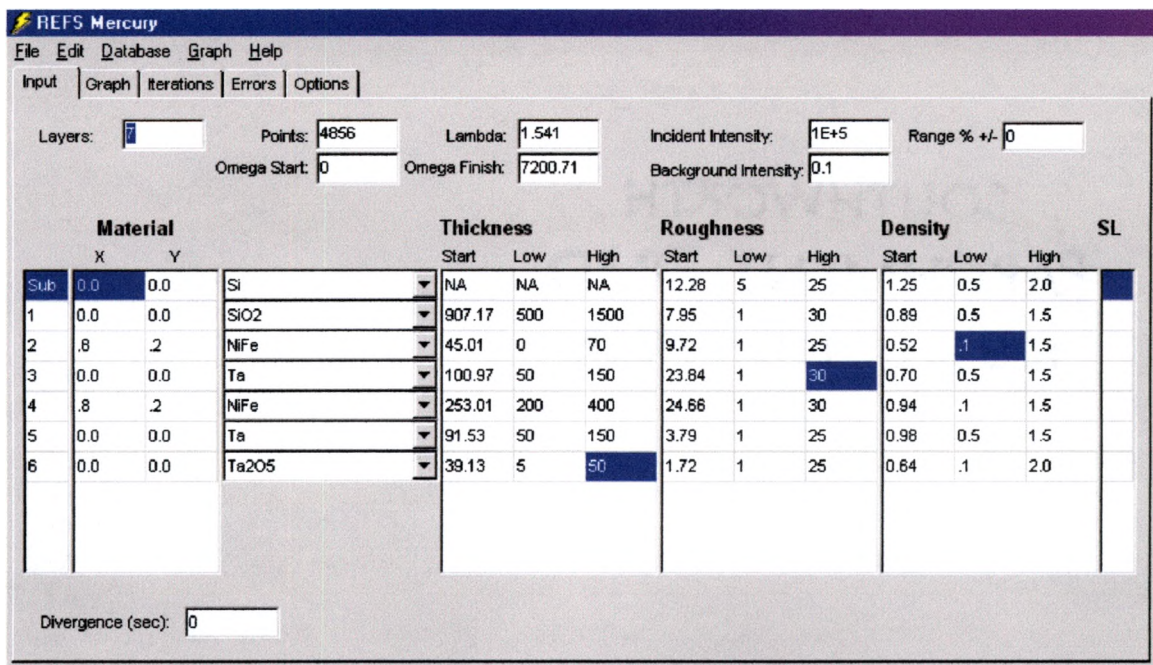


Figure 53 This is a screen shot of REFS Mercury Software Shows model that was used to fit sample SWT 1-5 this has constraints on the Ta layers of 100A thick

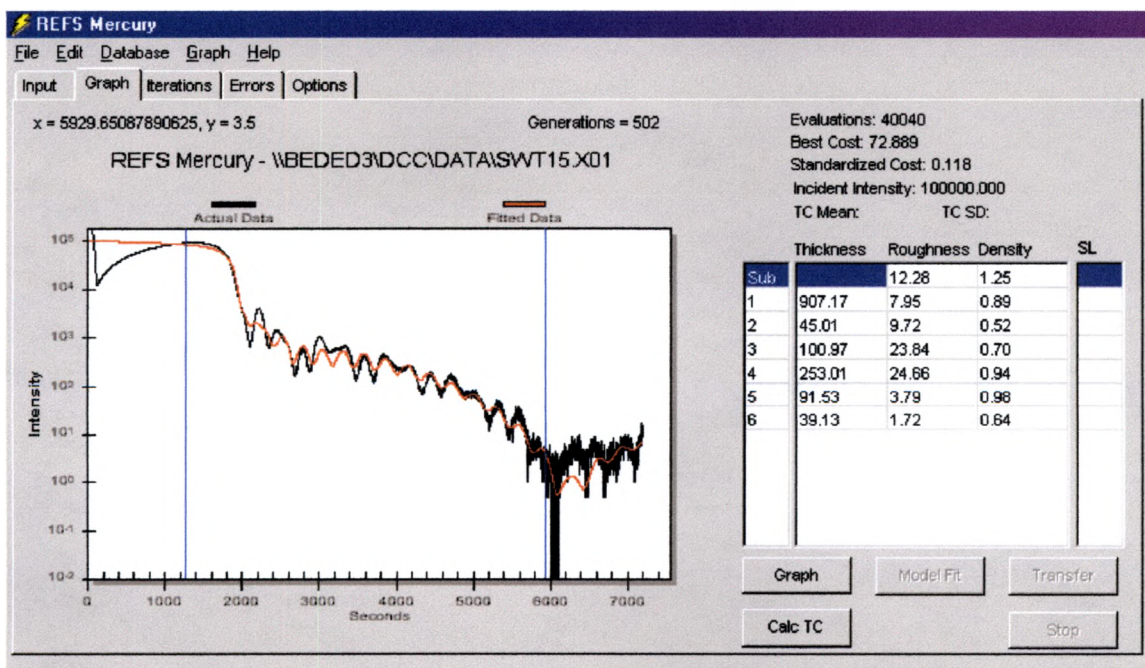


Figure 54 Screen Shot of REFS Mercury fitting the XRR data of SWT 1-5 with Constraints on the Ta layers

**REFS Mercury**  
 File Edit Database Graph Help  
 Input Graph Iterations Errors Options

Layers: 7 Points: 4856 Lambda: 1.541 Incident Intensity: 2E+5 Range % +/- 0  
 Omega Start: 0 Omega Finish: 7200.71 Background Intensity: 0.1

Sub	Material		Thickness			Roughness			Density			SL		
	X	Y	Start	Low	High	Start	Low	High	Start	Low	High			
Sub	0.0	0.0	Si	NA	NA	NA	NA	NA	15.48	5	25	1.42	.1	2.0
1	0.0	0.0	SiO2	798.40	500	1500	16.50	1	30	0.87	0.5	2.0		
2	.8	.2	NiFe	46.47	0	70	18.53	1	25	0.58	.1	1.5		
3	0.0	0.0	Ta	87.07	80	120	9.01	1	30	0.62	0.5	1.5		
4	.8	.2	NiFe	298.40	150	400	1.22	1	30	0.69	.1	1.5		
5	0.0	0.0	Ta	96.58	80	120	1.30	1	25	0.93	0.5	1.5		
6	0.0	0.0	Ta2O5	40.01	5	50	4.02	1	25	1.29	.1	2.0		

Divergence (sec): 0

**Figure 55** This is a screen shot of REFS Mercury Software Shows model that was used to fit sample SWT 1-6

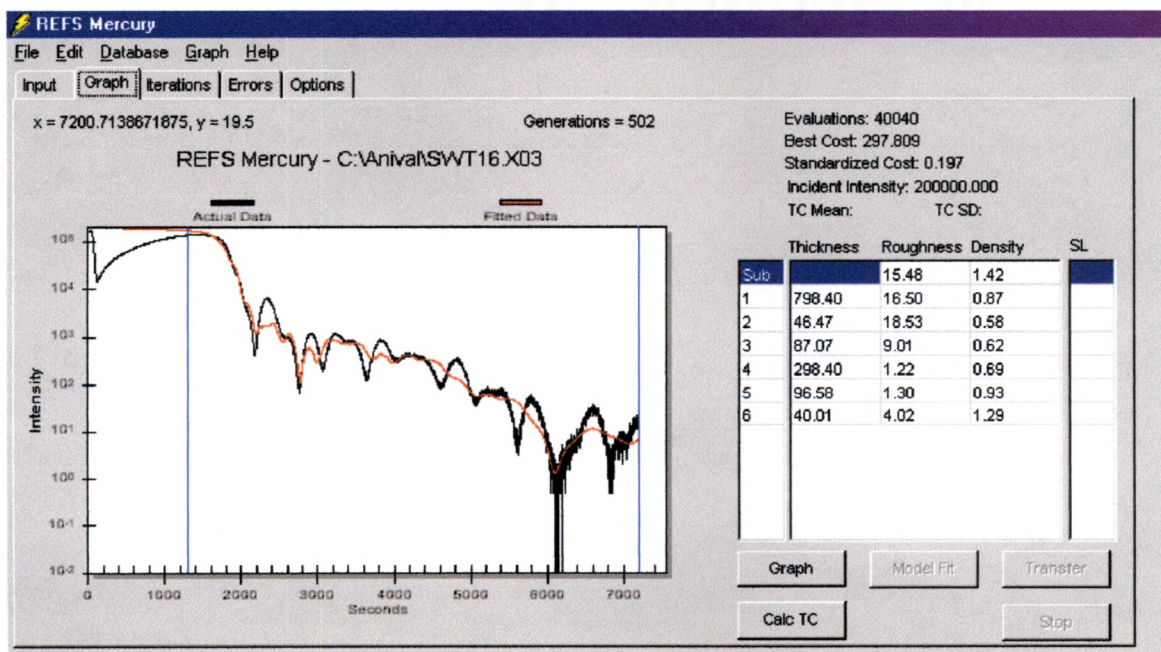


**Figure 56** Screen Shot of REFS Mercury fitting the XRR data of SWT 1-6

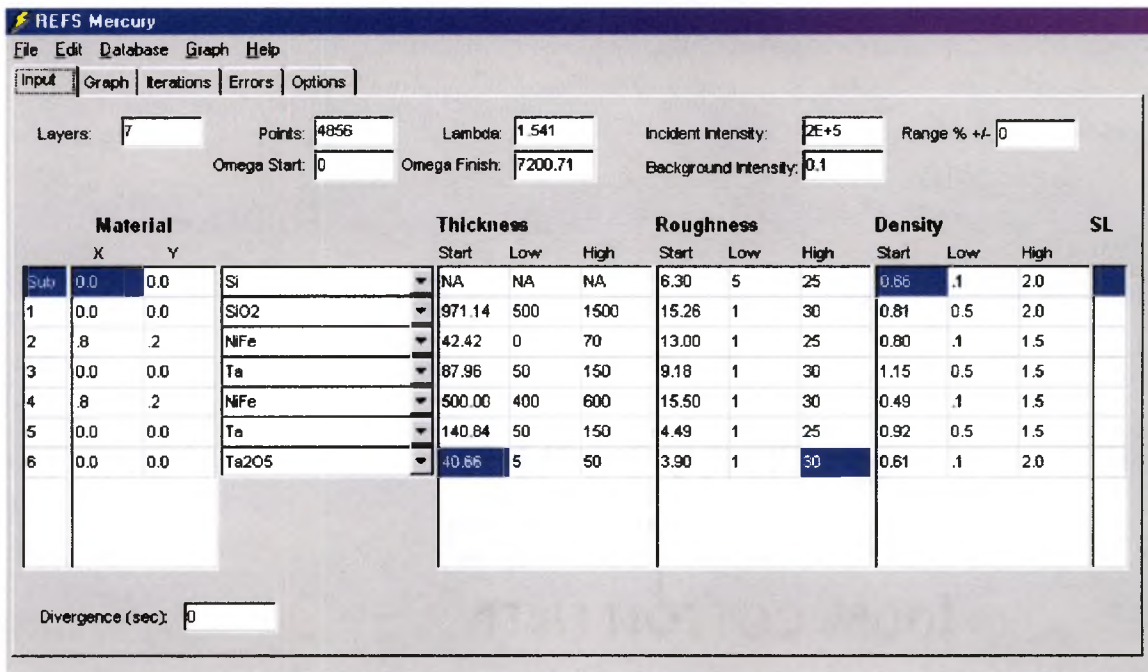


Figure 57 This is a screen shot of REFS Mercury Software Shows model that was used to fit sample SWT 1-7

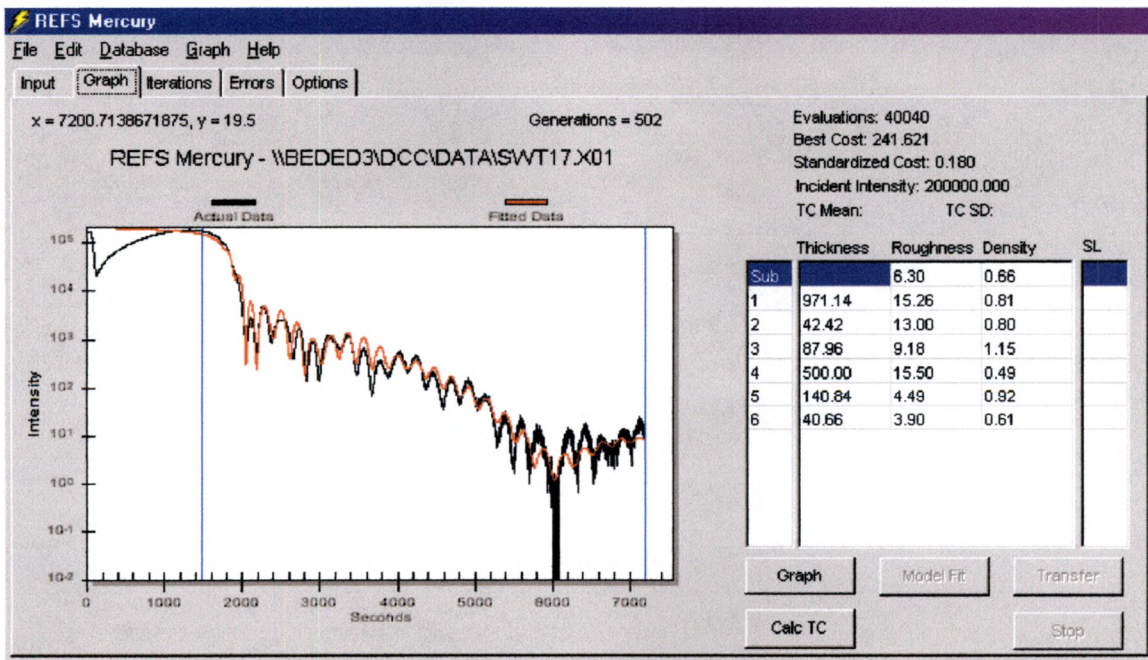


Figure 58 Screen Shot of REFS Mercury fitting the XRR data of SWT 1-7

## CHAPTER 5

### CONCLUSION

In conclusion, my thesis demonstrated examples of how x-ray analysis methods can be used for better understanding of ULSI and magnetic film materials. By using the three techniques of Powder Diffraction, Grazing Incident X-ray Diffraction and X-ray Reflectivity, a more complete understanding of the film materials is possible. Powder X-ray Diffraction shows what the crystal phase is present in the thin film and can also give you information on the order, if it is single crystalline or textured polycrystalline. When powder diffraction cannot detect useful information Grazing Incidence X-ray Diffraction can be used too more sensitively analyze the film. GIXRD can be use for thin polycrystalline film material due to the small angle of incidences with the beam, which minimizes substrate interference. This technique gives you information on the crystal phase and the texture of the film. By using both powder diffraction and GIXRD you can either confirm or disprove the film characterization. The ever-decreasing size of the ULSI devices is making GIXRD very important for film characterization. Using the XRR technique and along with the Bede RADS Mercury software you can get very accurate measurements of the film thickness and surface and interfacial roughness for the fitting program regardless of film crystallinity or amorphousness. Along with the thickness and roughness the software gives you a loose estimate of what the density of

each film as compared to the bulk material, which can be very useful. Also in my thesis I mentioned two deposition systems that were used to grow the test films.

In my data I was able to identify most of the material used in each film. In some cases I was not able to identify the material. For example, the SWT 1-5 GIXRD data shows that Tantalum is present but no Permalloy. Also there were two mystery peaks that I could not identify the peaks given the information about the films since any of the materials present in the films do not have any diffraction peaks lower than 38 degrees. In those cases I believe that the material present had very little crystalline portion which maybe means that the material was more amorphous than crystalline. However, note that my analysis of thick Cu films indicated that Cu  $K\alpha_1$  is not a sensitive probe for Cu diffraction peaks. I was able to use both techniques to confirm the peaks on a couple of the films. Then there were a couple of films like the AlCu film from Lucent Technologies where the GIXRD confirmed without a doubt that it was Al and that it was polycrystalline with texture. From the XRR data I was able to get a good fit and a very good measurement of the thickness and roughness.

The films that I studied are just a few materials used to in making ULSI devices. Other ULSI materials can also be analyzed this way. For example Cu, NiSi, Poly Si, can be analyzed with x-rays. The three techniques do not completely analyze ULSI film materials, but they do give you a very useful understanding of their structure.

## APPENDIX A

### Powder Diffraction Outline Procedures

Theta/2 Theta measurement with both zccc's out of the way

X-ray tube Setting: 10 milliamperes 30 kilovolts

Beam condition: Nickel filter, smallest vertical slit at the second zccc shield, no zcccs

Detector: Parallel beam stage, smallest vertical slit on the detector holder, no parallel slits

1. Move the sample out of the way of the beam
2. Check if the detector is centered on the beam and set it to that position to find relative max intensity of the x-rays
3. Move the sample halfway into the beam by cutting the x-ray intensity in half
4. Rotate axis 2 to maximize the intensity of the beam.
5. Move the sample back out of the x-rays and then move back to cut the beam intensity in half
6. The sample is now parallel with the beam
7. Now it depends on your sample after this step
8. For quartz you can just start a scan but for the silicon wafer we grow on you need to find the 004 peak
9. Move detector out to 69.1 degrees
10. Move the sample to half that angle to 34.564 degrees
11. Use Rotary 2 to find the top of the Si(004) peak
12. Use Gonio 2 to optimize the tilt of the Si(004) peak. You are limited on this motor due to the hardware limit.
13. You might have to move the detector a little to find the peak
14. Then calibrate the linked motor TH/2TH D to 69.1 degrees
15. Now you are ready to start a scan
16. You might want to offset the linked motor by 2 degrees away from the Si peak since the peak intensity is higher than most peaks you are trying to find from your sample

## APPENDIX B

### Procedures for Parallel Beam X-ray Diffraction

Parallel Beam measurement with both zccc's out of the way.

X-ray tube Setting:

Alignment:	10 milli-amperes	30 kilovolts
Scan:	40 milli-amperes	50 kilovolts

Beam condition: Nickel filter, vertical slit on the second zccc scatter shield

Detector: Parallel slit in front of the detector, no slit on either side to the parallel slits

1. First check if the Parallel slits are in front of the detector you may also have to put a piece of aluminum in front of the parallel slits to avoid saturation of the detector.
2. If not move the slits to 30 mm and this should put the slit in front of the detector
3. Then move sample of way from the x-ray beam
4. Center the detector on the x-ray beam
5. Once the detector is centered on the x-ray beam move the sample into the beam where the intensity is cut in half.
6. Once the intensity is cut in half rotate Axis 2 to maximize the intensity of the x-rays
7. When you reach a max then move sample out from the beam and then begin to move the sample back into the beam to half the intensity
8. Now you should have the sample parallel to the beam.
9. For this measurement the only real moving part is the detector
10. But you have to remember that the sample needs to be rotated to 1 degree, which is 3600 arc-seconds on Axis 2 after sample is parallel to beam.
11. Then you can start your scan and you need to turn the power of the tube up to scan x-ray tube settings of: 40 milli-amperes      50 kilovolts
12. You have two options when starting you scan either a single scan or a looped scan
13. Single scan just set the range of the detector to about 50 degrees and start it from 20 degrees.
14. If you loop the scan you can do several scan all at one time.
15. When looped it should be set to do three scans where the sample is at 1, 1.5, 2 degrees and on each the detector will scan a 50 degrees range starting at 20 degrees.

## **Publications**

Metastable Permalloy monoxides based Spin valves and Pseudo-spin valves. Journal of Applied Physics. Issue April 15, 1999. Vol. 85 No. 8 pg. 6121.

The Magnetic and Structural Properties of Metallic and Nitride-Doped ( $\text{Co}_{90}\text{Fe}_{10}/\text{Cu}$ ) Multilayers. IEEE Transactions on Magnetics, Vol. 33 No. 5, Sept. 1997 pg. 3664.

Ti/TiN Coatings for Microfabricated Cantilevers used in Atomic Force Microscopy. Journal of Vacuum Science Technology B., Vol 18 No. 3, May/June 2000 pg. 1182.

**CP# 20135** "Novellus Tungsten Fault Detection Using Semy and Silverbox SI Automation, Semy and AMD". Has not yet been Published.

## BIBLIORAPHY

- [1] D.K. Bowen and B.K. Tanner, High Resolution X-ray Diffractometry and Topography (Taylor & Francis Inc., Bristol, 1998).
- [2] Bede Scientific Instruments Operation Manual, Reflectivity Stimulation, May 1993
- [3] B.D. Cullity, Elements of X-ray Diffraction (Addison-Wesley Publishing Company, Inc., Reading, 1956).
- [4] R. Jenkins and R.L. Snyder, Introduction to X-ray Powder Diffractometry (John Wiley & Sons, Inc., New York, 1996).
- [5] S.A. Campbell, The Science and Engineering of Microelectronic Fabrication (Oxford University Press, Inc., New York, 1996).
- [6] W.R. Runyan and K.E. Bean, Semiconductor Intergrated Circuit Processing Technology (Addison-Wesley Publishing Company, Inc., 1990).
- [7] B.E. Warren, X-ray Diffraction (Dover Publication, Inc , New York, 1990).
- [8] R.W. Dail, X-Ray Diffraction and Magnetometric Study of Sputtered Metal Thin Films (Southwest Texas State Univeristy Publishing, San Marcos, 1996).
- [9] R. Selestino, Fabrication and Analysis of Ferromagnetic Cobalt Iron Metal Alloy Multilayers (Southwest Texas State University Publishing, San Marcos, 1998).
- [10] R.K. Waits, Thin Film Desposition and Pattering (Published by the America Vacuum Society, New York, 1998).
- [11] G. Lim, Journal of Material Research **2**, 471 (1987).
- [12] D.K. Bowen, Material of Research Society **208**, 113 (1991)

## Vita

Anival Grabiél Ayala was born in Carizo Springs, TX on January 15, 1975, the son of Victor Ayala and Noelia Ayala. After completing high school at Sam Rayburn in Pasadena, TX in 1993 he entered Southwest Texas State University in San Marcos, TX. While at Southwest Texas State he was able to work under Dr. Carlos Gutierrez in the Physics Department and do research. From the research he was able to get published in two journals as co-authors. He received his Bachelor of Science from Southwest Texas State University in the May of 1998. He then entered the Graduate program at Southwest Texas State University in the Physics Department.

Permanent Address:                      2107 Blueberry  
   Pasadena, TX 77502

This Thesis was typed by Anival Grabiél Ayala